University of Tennessee, Knoxville
TRACE: Tennessee Research and Creative Exchange

Masters Theses | Graduate School

8-2010

Radioisotopic Impurities in Promethium-147 Produced at the ORNL High Flux Isotope Reactor

James Howard Hinderer
University of Tennessee - Knoxville, jhindere@utk.edu

Follow this and additional works at: https://trace.tennessee.edu/utk_gradthes

 Part of the Nuclear Engineering Commons

Recommended Citation

Hinderer, James Howard, "Radioisotopic Impurities in Promethium-147 Produced at the ORNL High Flux Isotope Reactor. " Master's Thesis, University of Tennessee, 2010.
https://trace.tennessee.edu/utk_gradthes/717

This Thesis is brought to you for free and open access by the Graduate School at TRACE: Tennessee Research and Creative Exchange. It has been accepted for inclusion in Masters Theses by an authorized administrator of TRACE: Tennessee Research and Creative Exchange. For more information, please contact trace@utk.edu.

www.manaraa.com

To the Graduate Council:

I am submitting herewith a thesis written by James Howard Hinderer entitled "Radioisotopic Impurities in Promethium-147 Produced at the ORNL High Flux Isotope Reactor." I have examined the final electronic copy of this thesis for form and content and recommend that it be accepted in partial fulfillment of the requirements for the degree of Master of Science, with a major in Nuclear Engineering.

Lawrence H. Heilbronn, Major Professor

We have read this thesis and recommend its acceptance:

Lawrence W. Townsend, Laurence F. Miller

Accepted for the Council:
Carolyn R. Hodges

Vice Provost and Dean of the Graduate School

(Original signatures are on file with official student records.)

www.manaraa.com

To the Graduate Council:

I am submitting herewith a thesis written by James H. Hinderer entitled "Radioisotopic Impurities in Promethium-147 Produced at the ORNL High Flux Isotope Reactor." I have examined the final electronic copy of this thesis for form and content and recommend that it be accepted in partial fulfillment of the requirements for the degree of Master of Science with a major in Nuclear Engineering.

Lawrence H. Heilbronn

We have read this thesis
and recommend its acceptance:

Lawrence W. Townsend

Laurence F. Miller

Accepted for the Council:

Carolyn R. Hodges
Vice Provost and Dean of the Graduate School

www.manaraa.com

Radioisotopic Impurities in Promethium-147 Produced at the ORNL High Flux Isotope Reactor

A Thesis
Presented for partial fulfillment of requirements for the
Master of Science
Degree
The University of Tennessee, Knoxville

James Howard Hinderer
August 2010

www.manaraa.com

ACKNOWLEDGEMENTS

I would like to thank Dr. Lawrence Heilbronn for serving as my faculty advisor and supporting this project. This research was conducted under the Isotope Development Group at the Oak Ridge National Laboratory (ORNL). I would like to thank Dr. Russ Knapp for sponsoring me and to the rest of the staff for their support - with special thanks to Dr. Saed Mirzadeh who guided me throughout the course of this research.

www.manaraa.com

ABSTRACT

There is an intense interest in the availability of radioactive isotopes that could be developed into nuclear batteries. Promethium-147 is one of the isotopes of interest for use in nuclear batteries as well as in other compact low power applications. Pm-147 is a pure beta (β^-) emitter with a half-life of 2.62 years. For this research, Pm-147 was produced from enriched Nd-146 via the neutron capture method in the Hydraulic Tube facility of HFIR at the Oak Ridge National Laboratory.

Radioisotopic impurities produced via the neutron capture method have significant effects on its potential final use for nuclear battery applications. This research provides information on the co-production levels of the radioisotopic impurities in the samples containing Pm-147 and their effects on the required shielding. Gamma spectroscopy analysis served as the primary method in the evaluation of the impurities. Previous research had identified the presence of these impurities but it had not studied them in detail.

www.manaraa.com

TABLE OF CONTENTS

Chapter Page

1. **INTRODUCTION, PURPOSE, AND SCOPE ……..…… 1**

2. **LITERATURE REVIEW ……. 4**

3. **METHODS…….. ……... 21**

4. **RESULTS ……... 38**

5. **DISCUSSION OF RESULTS ……... 60**

6. **CONCLUSIONS AND FUTURE WORK……...…….. 66**

LIST OF REFERENCES ……....67

APPENDICES …… 70

APPENDIX A – FIGURES ……..... 71

APPENDIX B – TABLES …….. 88

VITA…….. 90

www.manaraa.com

LIST OF TABLES

Table Page

2.1 General Information on Promethium & Neodymium ……... 6

2.2 Properties of Isotopes Useful for Power Generation…….16

3.1 Nd-146 Material Batch Information…….....21

3.2 Nd-146 Target Batch Weights……..….25

3.3 Irradiation Schedules for Targets……...32

4.1 Summary of Impurities……..51

4.2 Error Percentages on Analyzed Peaks……55

4.3 Total Error for the Analyzed Gamma Peaks……57

4.4 Calculations for Samples NM-765T and -765B Radioactivity …….……88

4.5 Calculations for Sample NM-668 Radioactivity…….88

4.6 Shield Calculation Results for NM-668…….89

4.7 Lead Shielding Calculation Parameters for NM-668……...89

www.manaraa.com

LIST OF FIGURES

Figure		Page
3.1	Hydraulic Tube Capsule Assembly	23
3.2	Quartz Ampoules in Aluminum Foil	25
3.3	Schematic of the HFIR Flux Trap	30
3.4	Aliquot of Sample NM-668	34
3.5	Sample NM-765T	35
3.6	Gamma Spectrometer Efficiency Curves	37
4.1	Gamma Spectrum of NM-668 – 81 Days from EOB	39
4.2	LOG Plot of Gamma Spectrum: NM-668 – 81 Days from EOB	40
4.3	Gamma Spectrum of NM-668 – 221 Days from EOB	41
4.4	Gamma Spectrum of NM-668: Channel 0-175	42
4.5	Gamma Spectrum of NM-668: Channel 150-550	43
4.6	Gamma Spectrum of NM-668: Channel 340-650	44
4.7	Gamma Spectrum of NM-668: Channel 550-1000	45
4.8	Gamma Spectrum of NM-668: Channel 925-1025	46
4.9	Gamma Spectrum of NM-668: Channel 1000-1070	47
4.10	Gamma Spectrum of NM-668: Channel 1050-1500	48
4.11	Gamma Spectrum of NM-668: Channel 1350-4097	49
4.12	Dose Rates of Lead Shielding for NM-668	54
4.13	Gamma Spectrum of NM-765T	71
4.14	LOG Plot of Gamma Spectrum for NM-765T	72

www.manaraa.com

LIST OF FIGURES (cont.)

Figure Page

4.15 Gamma Spectrum of NM-765T – Channel 0-175……..…73

4.16 Gamma Spectrum of NM-765T – Channel 150-550…….……74

4.17 Gamma Spectrum of NM-765T – Channel 340-650....…….……75

4.18 Gamma Spectrum of NM-765T – Channel 550-1000…..…….……76

4.19 Gamma Spectrum of NM-765T – Channel 1000-1070…….……77

4.20 Gamma Spectrum of NM-765T – Channel 1050-1500…….……78

4.21 Gamma Spectrum of NM-765T – Channel 1350-2800…….……79

4.22 Gamma Spectrum of NM-765B ……...…….……80

4.23 Gamma Spectrum of NM-765B – Channel 0-175…….……81

4.24 Gamma Spectrum of NM-765B – Channel 150-550....…….……82

4.25 Gamma Spectrum of NM-765B – Channel 340-650..…..…….……83

4.26 Gamma Spectrum of NM-765B – Channel 550-1000……..…….……84

4.27 Gamma Spectrum of NM-765B – Channel 1000-1070…….……85

4.28 Gamma Spectrum of NM-765B – Channel 1050-1500…….……86

4.29 Gamma Spectrum: NM-765B – Channel 1350-2800…….……..87

5.1 Sample NM-668 - Activity of Nd-147…….……..61

www.manaraa.com

CHAPTER 1

INTRODUCTION, PURPOSE, AND SCOPE

1.1 INTRODUCTION

There is an intense interest in the availability of the low energy beta-emitting promethium-147 (Pm-147) radioactive isotope for use in nuclear batteries as well as other compact low power applications. Promethium is an element of the rare-earth group that is not found in nature [1]. All the isotopes of promethium are radioactive. Investigations into the uses of the element have shown the possibility of utilizing Pm-147 as a nuclear battery [1, 3]. Pm-147 has a half-life of 2.62 years. Nuclear batteries use the emission of ionizing radiation to generate electrical power. Promethium-147 is a soft beta emitter with the emission of only one low abundant gamma photon, thus making it a good candidate for a nuclear battery.

Promethium-147 is a fission product and traditionally, it was isolated in large amounts from the fission of uranium-235 by the reprocessing of the spent fuel. In the late 1970s, the Oak Ridge National Laboratory (ORNL) possessed approximately 853 grams of Pm-147 which had been isolated from fission products at the Hanford, Washington nuclear processing facility. This inventory has been completely exhausted. Alternatively, Pm-147 can be produced by bombarding highly enriched Nd-146 in a nuclear reactor via the following reaction (commonly referred to as “neutron capture route”):

www.manaraa.com

$$^{146}Nd[n,\gamma]\ ^{147}Nd(t_{1/2}=11d,\ \beta^{-}) \longrightarrow ^{147}Pm$$

This research provides information on the co-production levels of radioisotopic impurities in the samples containing Pm-147 produced at the HFIR and their effects on the required shielding. Previous research had identified the presence of these impurities but it had not studied the impurities in detail.

1.2 PURPOSE

The immediate goal is to study the radioisotopic impurities, which are co-produced in the Pm-147, produced by the neutron capture route and their effects on the required shielding. An evaluation of the radioistopic impurities as a result of the data collected from the irradiated samples of Neodymium-146 (Nd-146) material will provide valuable information required for the future development of Pm-147 for low power applications.

1.3 SCOPE

This project utilized the High Flux Isotope Reactor (HFIR) at the Oak Ridge National Laboratory (ORNL) to produce the Pm-147. The major elements of the research included the following:

www.manaraa.com

1. Preparation of a series of small highly enriched Nd-146 targets
2. Irradiation of the targets in the HFIR Hydraulic Tube (HT) Facility
3. Some tracer level processing and separation techniques
4. Analysis of the radionuclide impurity levels using γ-ray spectroscopy

Gamma spectroscopy analysis served as the primary method in the evaluation of the radioisotopic impurities in the Pm-147.

www.manaraa.com

CHAPTER 2

LITERATURE REVIEW

2.1 Existence and Production of Promethium-147

Promethium, element 61 on the periodic table, is an element of the rare-earth group that is not found in nature. Although research in the early twentieth century predicted the presence of an element between neodymium and samarium, promethium was not first produced until 1946 when Jacob A. Marinsky, Lawrence E. Glendenin and Charles D. Coryell were analyzing by-products of uranium fission at the Oak Ridge National Laboratory [1]. Promethium has seventeen known isotopes (all radioactive), ranging in atomic masses from 134 to 155. Pm-145 is the longest lived isotope with a half-life of 17.7 years and with a specific activity of 940 Ci/g. Pm-147 is a pure beta (β^-) emitter with a half-life of 2.62 years and it is regarded as the most useful of the isotopes [2].

Pm-147 can be obtained two different ways: (1) Isolation of Pm-147 in Uranium-235 fission products and (2) Neutron irradiation of neodymium-146. Traditionally, Pm-147 was isolated in large amounts from the fission of uranium-235 by the reprocessing of the spent fuel. According to Lee [4], approximately 85 curies of Pm-147 is present in one kilogram of uranium metal for a 30,000 MWD/T burn-up level of spent fuel.

www.manaraa.com

Since fission products can no longer be processed in the United States, the only effective alternative for producing Pm-147 is via thermal neutron bombardment of Nd-146. Nd-146 is a stable isotope of the rare earth element neodymium, which has a natural abundance of 17% [1]. The irradiation of Nd-146 yields Nd-147 which decays through beta emission to Pm-147 is illustrated below:

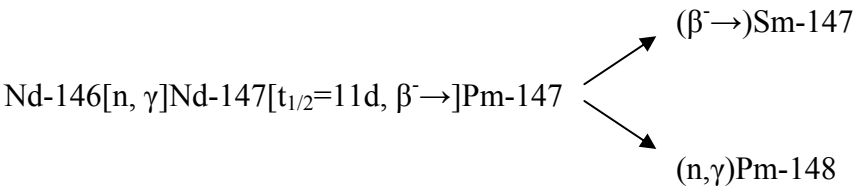

Nd-147 decays to Pm-147 100% of the time with a decay energy of 896 keV, while the Pm-147 decays to stable samarium-147 (Sm-147) approximately 99.994% of the time [1]. The decay of Pm-147 is followed by the emission of an extremely weak γ-ray at 121 keV with an intensity of only 0.00285%. The maximum energy of the beta particles emitted from Pm-147 is 224.5 keV, with an average energy of ~62 keV [3].

This method of neutron bombardment is simple and results in low specific activity; however, isotopic contaminants in the Pm-147 produced via neutron capture have significant effects on its potential final use for nuclear battery applications. Specifically, promethium-148 (Pm-148), formed by the subsequent neutron capture of Pm-147, is the main concern since it emits penetrating γ-rays at 288 keV, 414 keV, and 550 keV, as seen below in Table 2.1 [19].

www.manaraa.com

TABLE 2.1 General Information on Promethium & Neodymium

		γ-rays		Average β^-	
Isotope	Half-Life	Energy (keV)	Intensity (%)	Energy (keV)	Decay Product
Nd-147	10.98 days	91	28	233	Pm-147
		531	13		
Pm-147	2.62 years	121	0.00285	62	Sm-147
Pm-148	41.3 days	288	12.5	149	Sm-148
		414	18.7		
		550	18.7		

2.2 General Theory of Radioactive Decay and Transmutation

According to Turner [5], "the rate of decay, or transformation, of a radionuclide is described by its activity, that is, by the number of atoms that decay per unit time." The activity of a radionuclide decreases exponentially as seen in equation 2.1 below (assuming no production during the decay):

$$\frac{dN}{dt} = -\lambda N \qquad (2.1)$$

where, N = number of atoms

λ = decay constant = $\frac{\ln 2}{t_{1/2}}$

$t_{1/2}$ = half life of the radionuclide in unit time

www.manaraa.com

By separating the variables in equation 2.1 and integrating on both sides of the equation, the following expression describes the exponential decay law [5]:

$$N(t) = N_0 e^{-\lambda t} \qquad (2.2)$$

where, N_0 = the number of atoms of the radionuclide present at time t=0

N(t) = number of parent radionuclide at time = t

The daughter product is formed at the rate the parent decays. If the daughter product is radioactive, then it decays to another daughter product creating a decay chain. This is seen in the following expression [5]:

$$\frac{dN_2}{dt} = -\lambda_1 N_1 - \lambda_2 N_2 \qquad (2.3)$$

As the size of the decay chain increases (3 or greater member chain), the equations get complicated and the differential equation is much more difficult to solve. The Bateman equations are a general solution for an n-member chain of nuclear transmutations ($N_1 \rightarrow N_2 \rightarrow \ldots \rightarrow N_n$) and is represented in the following expression [14]:

$$N_n = C_1 e^{-\lambda_1 t} + C_2 e^{-\lambda_2 t} + ... + C_n e^{-\lambda_n t} \qquad (2.4)$$

www.manaraa.com

where $C_1 = \dfrac{\lambda_1 \lambda_2 \cdots \lambda_{n-1}}{(\lambda_2 - \lambda_1)(\lambda_3 - \lambda_1)\cdots(\lambda_n - \lambda_1)} N_1^0$

$$C_2 = \frac{\lambda_1 \lambda_2 \cdots \lambda_{n-1}}{(\lambda_1 - \lambda_2)(\lambda_3 - \lambda_2)\cdots(\lambda_n - \lambda_2)} N_1^0$$

$$\vdots$$

$$C_n$$

Radioactive decay in a nuclear reactor is similar to simple decay, with the additions of the neutron cross section of the material and the neutron flux of the reactor [13]:

$$\frac{dN}{dt} = decay - transmutation$$

$$\frac{dN}{dt} = -\lambda N - \sigma\phi N$$

$$\frac{dN}{dt} = -(\lambda + \sigma\phi)N$$

$$\frac{dN}{dt} = -\Lambda N$$

where: $\sigma =$ neutron absorption cross section (barnes)

$\phi =$ neutron flux (n cm^{-2} sec^{-1})

Finally arriving at the following equation:

$$N(t) = N_0 e^{-\Lambda t} \qquad (2.5)$$

www.manaraa.com

2.2.1 Growth of Radioactive Products

If the parent of the radioactive pairs (parent-daughter combination) is shorter-lived than the daughter ($\lambda_1 > \lambda_2$), which is such the case for the Nd-147→Pm-147 pair, then there is no evidence of radioactive equilibrium [13]. Initially, the parent decays as the amount of the daughter product rises; however, after a certain period of time (~10 half-lifes of the parent), the remaining decay will be completely characteristic with the half-life of the daughter product. The number of atoms for the daughter product can be calculated by the following expression:

$$N_2(t) = \frac{\lambda_1}{\lambda_2 - \lambda_1} N_1^0 e^{-\lambda_1 t} \qquad (2.6)$$

Where: N_1^0 = initial number of atoms of the parent

By factoring in the condition for the initial activity of the daughter product, A_2^0, the activity of the daughter product, A_2, at any time can be calculated by the following expression [13]:

$$A_2 = \frac{\lambda_2}{\lambda_2 - \lambda_1} A_1^0 (e^{-\lambda_1 t} - e^{-\lambda_2 t}) + A_2^0 e^{-\lambda_2 t} \qquad (2.7)$$

www.manaraa.com

Where A_2^0 = activity of daughter at time = 0

Investigating the decay of Nd-147, Rangacharyulu et al. (1974) determined an experimental level scheme for Pm-147 which included γ-rays at 182, 228.5, 275, 319.5 and 725 keV [22]. According to Rangacharyulu, "the 39 and 43 keV X-rays from Pm-147 are expected to appear in all the sum-coincidence spectra and to add up with the γ-ray component satisfying the sum-gate condition. Obviously, their presence is ignored while assigning observed γ-ray transitions in the decay scheme." [22]

2.2.2 HFIR Neutron Flux

Neutrons are organized according to their energy levels and, subsequently, velocities in fission reactors. Thermal neutrons have an average energy of 0.025 eV and a mean velocity of 2,200 meters per second. Epithermal neutrons range in energies from 1 eV to 1 MeV while fast neutrons are greater than 1 MeV as they retain much of the energy following fission. Fast neutrons contribute very little to the [n, γ] reaction, but instead induce reactions such as [n,p], [n,n'], and [n,2n] [18].

In 1995 Mahmood and Mirzadeh performed a series of experiments to characterize the neutron dosimetry of the HFIR Hydraulic Tube (HT) Facility [15]. They used a variety of flux monitors to measure the total, fast and thermal neutron fluxes at five different

www.manaraa.com

positions in the HT. Their results indicated the thermal-to-fast flux ratio varied from about 5.4 at the center position to 6.7 at the ends [15]. This information indicates approximately 15% to 20% of the neutrons are fast while the rest are thermal neutrons. The HFIR HT facility configuration is described in detail in section 3.3.

2.3 Purification Techniques for the Separation of Nd-147/Pm-147

Although the neutron bombardment method produces much lower quantities of Pm-147 and has further complication that the neodymium target material must be recovered, the levels produced are still useful. A chromatographic extraction method for the production and purification of Pm-147 was patented by researchers under-which this study was conducted. This technique involves dissolving the HFIR irradiated enriched neodymium-146 material to form an acidic solution, loading the acidic solution onto an extraction chromatographic separation apparatus containing di(2-ethylhexyl)orthophosphoric acid (HDEHP), and finally chromatographically separating the promethium-147 from the neodymium-147 [4].

The experimental yield of the Pm-147 ranged from 123 to 959 μCi/mg of Nd-146 [4]. While this separation method was successful, the results also showed the presence of the following impurities: Promethium-148, Europium-152, -154, and -155, Gadolinium-153, Iridium-192, and Cobalt-60 [4].

www.manaraa.com

Quantifying the level of these impurities is the basis for this current investigation presented in this thesis.

2.4 Applications of Promethium-147

Pm-147 has multiple applications including use as a beta source for thickness gauges and as a source light through absorption by phosphor (as used in compact fluorescent light-bulbs). With a half-life of 2.6 years, Pm-147 is particularly useful for devices that require long-term dependable operation - such as auxiliary power sources for space probes or satellites.

As mentioned previously, Pm-147 is an ideal candidate for use as a nuclear battery due to its favorable power density and low biological hazard as a result of the emission of very few low-energy gamma photons. Nuclear batteries capture decay particles and transfer them into a usable electrical current. More specifically, the electrical current is created through a process called betavoltaics by which electrons normally lost due to the decay of radioactive isotopes are harnessed to create a steady stream of electricity. A semiconductor would be used to catch the flying electrons and to convert them into a steady power source. Such a battery, using Pm-147, would have a useful life of at least five years.

www.manaraa.com

In a report published in 1966, McKee investigated the economic feasibility of producing Pm-147 by irradiation of Nd-146 and found it to be less attractive when compared to using plutonium-238 sources. One of the contributing factors had to do with the high production costs of the Pm-147 including lower than desired product yields due to the presence of contaminants. Specifically, McKee indicates the presence of Pm-148 from the (n,γ) reaction and a small quantity of Pm-146 from the (n,2n) reaction from fast neutrons. According to McKee [1]:

> There may be no practical means for reducing the Pm-146 content although studies are in progress on selective burning out of this isotope by irradiation with thermal neutrons. The Pm-148 content can be reduced to a negligible amount by aging the Pm-147 for about one half-life or 2 and ½ years.

The radioactive contaminants give off other forms of radiation (gamma, alpha) that are harmful to the electronic components of the device and the humans handling it.

2.4.1 Construction of a Pm-147 Nuclear Battery

The nuclear battery was first discovered in the 1950s and was patented to Tracer Lab on March 3, 1959 [11]. According to Akhil [11], "even though the idea of was given more than 30 years before no significant progress was made on the subject because the yield was very less." The first prototype power, made from Strontium-90, cell produced

www.manaraa.com

100,000 times more energy per gram than the largest thermal battery yet in existence [11]. The concept is simple and is similar to that of solar photovoltaic energy – capture electric charges of the beta particles from the radionuclide and convert it to electricity. However, the application proved not to be so simple due to the low efficiency of the device resulting from the semiconductor failing to capture a majority of the electrons.

Flicker, Loferski, and Elleman [3] constructed the first Promehtium-147 atomic battery and shared the results in a study published in 1964. Pm-147 was chosen over a Strotonium-90 power source due to its lower radiation damage threshold. Strontium-90 emits high energy (up to 2 MeV) electrons that significantly degrade the power output and construction of the electrical device. The authors recognized a number of problems that had to be overcome in order to maximize the results of the battery prototype [3]:

> At the beginning of this study, it was clear that the following problems would have to be considered. 1) Both the efficiency of energy conversion via the electron-voltaic effect and the rate of radiation damage introduction would have to be measured for electrons whose energies corresponded to those present in the Pm^{147} spectrum. 2) The radiation from radioisotope impurities present in Pm^{147} as produced by the AEC had to be determined in order to establish an upper limit on the amount of such impurities which could be tolerated in the radioisotopic source. 3) A technique had to be developed for fabricating homogeneous Pm^{147} sources.

www.manaraa.com

The second problem for the authors is the same basis of this experiment, which is to comprehensively characterize the radioisotopic impurities in the Pm-147 material. The difference between this research and the research of Flicker et al. is that the Pm-147 was directly obtained from spent reactor fuel for Flicker's battery prototype development. In their case, 5 MeV alpha particles were emitted due to the presence of americium-241 (Am-241) in the source material. Flicker was able to reduce the alpha particle emission using various purification and separation techniques; however, the final device had to be designed to shield against the alpha particle energy in order to protect the electronics [3]. The presence of alpha particle emitters is of no concern for this study.

More recently, in 2008, Akhil pointed out that the semiconductors are improving and the world is on the verge of a nuclear battery renaissance. For example, a nuclear battery powered laptop computer called Xcell-N, which had been running continuously for the last eight months at the time of that published report (2008), is said to possess the capability to last five years! Table 2.2 shows a few of the potential radioisotopes that Ragheb identified in his paper entitled, "Radioisotopes Power Production" [12].

www.manaraa.com

Table 2.2: Properties of Isotopes Useful for Power Generation

Isotope (atomic no.)	Types of Radiation Emissions	Half-life	Specific Power (Watts/gram)
Tritium (3)	β-, no γ	12.3 y	0.26
Cobalt (60)	β-, γ	5.3 y	17.7
Nickel (63)	β-, no γ	100.1 y	0.02
Strontium (90)	β-, no γ	29 y	0.93
Promethium (147)	β-, few γ	2.6 y	0.33
Polonium (210)	A, few γ	136.4 d	144
Plutonium (238)	α, γ, SF	87.7 y	0.56

From Table 2.2, Strontium, Cobalt and Promethium are the most attractive candidates for nuclear batteries due to their high specific power and long half-lives.

Kavetskiy, Yakubova and others [27] recently constructed and tested a Pm-147 capacitor prototype. The direct charge promethium capacitor was made inside a vacuum enclosure with a length of 150 mm and an inner diameter of 54 mm. The prototype demonstrated an efficiency of 14% producing 140 μW of electrical power with a source activity of 2.6 Ci. The Kavetskiy and Yakubova study, completed in 2008, was the first to demonstrate the use of a radioactive isotope for electrical energy having greater than 10% conversion efficiency. All the others, including the state of the art Radioisotope Thermal Generator (RTG) that flew on the Cassini Mission to Saturn were less than 10% efficient [6].

www.manaraa.com

2.5 Calculation for the Exposure Rate from Gamma Emission

The quantity exposure, usually expressed in Roentgens (R) and given by the symbol X, is a defined as the extent of ionization events taking place when air is irradiated by ionizing gamma radiation [24]. The exposure rate expresses the rate of charge production per unit mass of air. The extent of the production of charged particles by photon interactions in air depends on the following factors: (1) the intensity of the radiations (fluence rate); (2) the energies of the photons; (3) the average fraction of the photon energy transferred to charged particles and available to be absorbed per photon interaction per unit mass – referred to as the mass energy absorption coefficient, μ_{en}/ρ; (4) the w-value for air which varies according to the humidity in air [25].

The fluence rate, φ, is determined by understanding the photons emitted from the source will pass uniformly through the surface of an imaginary sphere with a surface area of $4\pi r$ emitting S photons per second,

$$\varphi = \frac{S}{4\pi r^2} = \frac{Ay}{4\pi r^2} \tag{2.8}$$

Where: A = source activity

y = photon yield

www.manaraa.com

Multiplying the fluence rate by the photon energy will obtain the photon energy fluency rate, ψ [25]:

$$\psi = \frac{AyE}{4\pi r^2} \tag{2.9}$$

Where: E = photon energy

By multiplying both sides of the equation by the mass energy coefficient, μ_{en}/ρ, and applying all the appropriate conversion factors, the exposure is obtained [25]:

$$\dot{X} = 5.263x10^{-6} A\sum(y_i E_i(\mu_{en}/\rho)_i)/r^2 \qquad (\text{Gy h}^{-1}) \qquad (2.10)$$

2.6 Shielding of Gamma Radiation

The mass attenuation coefficients described in section 2.5 represents the probability of a photon interacting with a specified type of material independent of state of that material (solid, gas, etc.). In order to maximize the attenuation of these photons, the material (water, lead, etc.) must be designed to a certain thickness. At the moderate photon energies produced by the radioisotopic impurities in the promethium-147, Compton scattering occurs. These interactions scatter the gamma photons in different directions from the incident electrons and must be accounted for in the shielding design. The extent

www.manaraa.com

to which such secondary photons add to the dose is described through the use of an appropriate buildup factor [26].

The dose rate, D, at any point of interest outside the shield is given by the following expression [26]:

$$D = D_0 e^{-\mu x} \tag{2.11}$$

Where: D_0 = unshielded dose rate

μ = linear attenuation coefficient

x = thickness of shield

Assuming the radiation is emitted uniformly throughout the 4π geometry, allows the source to be treated as a point isotropic source. The primary dose rate incorporating a point isotropic source with buildup factor, B, is given by the following equation [26]:

$$\dot{D} = \frac{kSE\frac{\mu_{en}}{\rho}Be^{-\mu T}}{4\pi r^2} \tag{2.12}$$

Where k = conversion constant to convert fluence rate to dose rate

S = # of gamma rays per second

E = photon energy, MeV

μ_{en}/ρ = mass energy absorption constant

www.manaraa.com

T = thickness of shielding, cm

Equation 2.12 is useful to determine the dose rate if the shield thickness is known; however when the purpose is to determine the appropriate shielding thickness for a given dose rate then a more complex solution is required. An analytical form of the buildup factor can be incorporated into equation 2.12 and, through an iterative process using a computer or calculator, the desired shielding thickness can be calculated. One of the more popular methods for doing this is an expression referred to as Taylor's form of the buildup factor [26]:

$$B = A_1 e^{-\alpha_1 \mu T} + (1 - A_1) e^{-\alpha_2 \mu T} \tag{2.13}$$

A_1, α_1, and α_2 are constants for a given shield thickness and energy provided by Shultis and Faw [14]. By incorporating this expression for the buildup factor, the dose rate equation becomes [26]:

$$\dot{D} = \frac{k \sum_{i=1}^{n} S_i E_i \left(\frac{\mu_{en}}{\rho}\right)_i \left(A_1 e^{-(1+\alpha_1)\mu T} + (1 - A_1) e^{-(1+\alpha_2)\mu T}\right)_i}{4\pi r^2} \tag{2.14}$$

Equation 2.14 will be used to calculate and analyze the shielding thickness requirements as a function of the dose rates.

www.manaraa.com

CHAPTER 3

METHODS

3.1 Preparation of the Neodymium Targets

Two batches of enriched Nd-146 material in the form of Neodymium Oxide (Nd_2O_3) were used in this experiment. The material was obtained from the ORNL Inventory of Isotopes (see Table 3.1) for use in these experiments.

The distinguishing factor between the batches is the Nd-146 enrichment. These three batches were chosen because they had the highest Nd-146 assay available in the ORNL inventory. The enrichment level is critical to the conversion of the Nd-146 to Nd-147 via neutron bombardment thus minimizing the formation of impurities.

The aluminum capsules, also referred to as targets, were prepared using the ORNL Nuclear Medicine Group (NMG) procedure NMG49 - *Procedure for the Loading, Testing, Certification, and Irradiation of HFIR Hydraulic Tube Capsules.*

Table 3.1: Nd-146 Material Batch Information

Batch #	Form	Nd-146 Enrichment
161730	Nd_2O_3 - solid	86.84%
161701	Nd_2O_3 - solid	97.46%

www.manaraa.com

Adherence to the site procedures was important to ensure the quality assurance of the prepared specimens before irradiating them in HFIR. The data from the certification tests was compiled into the Experimental Authorization Basis Document (EABD) that was prepared for each aluminum capsule. The EABD had to be approved by a series of reviewers in order for the experiments to occur. Cloth gloves were worn at all times throughout the process of preparing the target capsules to prevent potential contaminants.

3.1.1 Quartz Ampoules

In order to reduce the potential of cross-contamination, the Nd was encapsulated inside a 6-millimeter O.D. synthetic quartz ampoule. Only one side of the ampoule was enclosed when beginning the preparation. The ampoule was first cleaned by immersing it in nitric acid for approximately 30 seconds and then rinsing it using de-ionized water. This process was completed multiple times for ampoules that would be used throughout the course of this experiment. All of the cleaned ampoules were placed on a fixture to hold them upright and the fixture was set inside of a sterile one-half pint beaker. The beaker was placed inside a laboratory oven 110 ± 5°C for 30 minutes. The ampoules were removed and placed inside a desiccator to dry using filtered air.

Two of the ampoules were removed from the desiccator to prepare one capsule. The cylindrically shaped capsule is made according the engineering drawing in Figure 3.1

www.manaraa.com

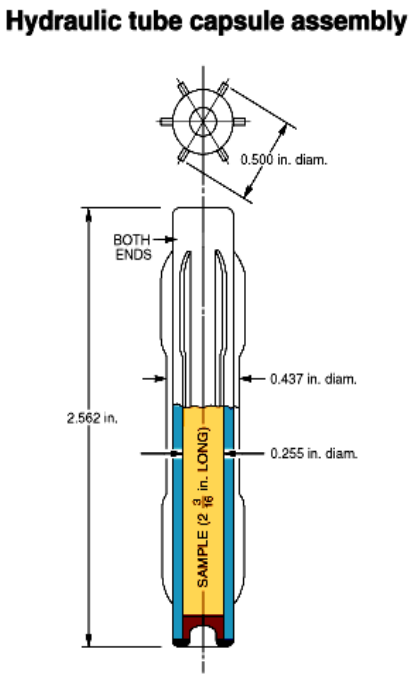

Figure 3.1: Hydraulic Tube Capsule Assembly

using finned tubing of aluminum 6061 [15]. Each capsule (or target) can hold up to two ampoules, while each ampoule holds only a small amount of material (2 – 4 milligrams).

Each aluminum target is assigned a unique identifier that is engraved into the side of it. This identifier is assigned in numerical order and according to the organization for which it is being tested. For instance, the nuclear medicine group, under which this study was conducted, is assigned set of identifiers beginning with the letters "NM."

www.manaraa.com

3.1.2 Loading of Material into Quartz Ampoules

The empty quartz ampoules were weighed individually using a calibrated laboratory scale with a sensitivity of 0.01 milligrams. Then, the enriched Nd-146 material (batch# 179801) was loaded into the quartz ampoules using a small stainless steel spatula. For the purpose of these experiments, only one to three milligrams of $^{146}Nd_2O_3$ was loaded into each ampoule. The weight of each ampoule with the sample in it was recorded and the difference in the two measurements gives the mass of the target material. The loaded, unsealed ampoules were placed in the oven at 110°C for at least 60 minutes. The samples were removed from the oven, allowed to cool to room temperature in a desiccator, and weighed again. If a difference exists between this weight measurement and one previously recorded, this is used in its place as the final. The ampoules were flamed sealed with a gas/oxygen flame. The flame was directed towards the region below the top opening in order to minimize the possibility of unburned gases from entering the ampoule. The sealed ampoules were stored in the desiccator until they were ready to be loaded into the aluminum capsule.

3.1.3 Aluminum Capsule Loading

The two quartz ampoules, containing Nd-146 samples, were first wrapped in 0.05 mm-thick aluminum foil (approximately four square inches) closely placed on top of each other with the flame sealed end pointing up as seen in Figure 3.2. Any excess aluminum

www.manaraa.com

Figure 3.2: Quartz Ampoules in Aluminum Foil

foil was removed. Since the two ampoules were from different batches and have different masses, the position of each was carefully documented. The aluminum foil serves as a positioning device so the quartz ampoules can be easily inserted and removed from the aluminum target.

A dime size piece of quartz wool was rolled into a ball and placed at the bottom of the sealed end of the aluminum capsule. The quartz wool was used as a cushion so that the ampoules would not slide around inside the capsule. The tightly wound aluminum foil containing the two targets was slid down into the aluminum capsule on top of the quartz wool with the flame sealed ends of the ampoules positioned upwards. The same dime size amount of quartz wool was placed at the top of the capsule before loosely sealing it with the end cap until the cap can be permanently welded in place.

www.manaraa.com

Table 3.2: Nd-146 Target Batch Weights

Target ID	Orientation of Ampoule in Capsule	Sample Mass (mg of Nd_2O_3)	Mass of Nd-146	Nd-146 Enrichment (%)
NM-668	only one ampoule	1.1	0.92	97.46%
NM-765	top	1.65	1.23	86.84%
	bottom	2.36	1.76	86.84%

Three targets containing a total of three ampoules, or samples, were irradiated and analyzed for this study (see information in Table 3.2). Target NM-765 contained two ampoules while target NM-668 only contained a single ampoule. NM-668 had been prepared for a previous study but was never irradiated.

The mass of the Nd-146 was calculated using both the atomic mass percentage of Nd-146 in the neodymium oxide as well as the assay percentage.

$$M_{Nd-146} = \frac{A_{Nd}}{A_{Nd} + A_O} \times M_{tot} \times E \qquad (3.1)$$

Where: A_{Nd} = atomic mass units of Nd_2 in Nd_2O_3 = 2*146 = 292 amu

A_O = atomic mass units of O_3 in Nd_2O_3 = 3*16 = 48 amu

M_{TOT} = total mass in milligrams of Nd_2O_3

E = Assay of Nd-146 = % Assay/100

www.manaraa.com

3.1.4 Welding of Aluminum Targets

The aluminum end cap was welded onto the target using a tungsten inert gas (TIG) welder in an inert glovebox. The procedure was completed by a certified welder. A weld inspection report was generated and was archived as part of the required documentation for the irradiation of the targets. The diameter was recorded and it read 11.17-mm (0.440 inches).

3.2 Testing and Certification of the Neodymium Target

Following the certified weld, each aluminum target underwent a series of certification tests:

- Helium Leak Tests
- Hydrostatic Pressure Test

The purpose of the tests was to verify the integrity of the capsules to ensure they do not leak during their irradiation cycles in the HFIR.

www.manaraa.com

3.2.1 Helium Leak Test

The helium leak test is to ensure the integrity of the weld of each aluminum target by checking for any leakage of the capsules. Each sealed aluminum target was first "bombed" with pure helium gas in a vacuum chamber. The target was sealed in a 6-inch diameter cylindrical vacuum chamber and pumped down to the minimum vacuum pump capacity. The vacuum valve was closed and the helium valve was opened. The helium pressurized the chamber to 120 psi and this pressure was held for 30 minutes. The vacuum chamber was vented and the aluminum capsule was removed wearing cloth gloves.

The capsule was then placed inside the helium leak detector test chamber mounted on the leak detector. The leak detector used was a Varian 959 system that had been recently calibrated. The leak detector contains a mass spectrometer that counts the helium ions. One capsule at a time was tested following the instructions in the vendor manual for operating the leak detector. Once the helium leak rate was recorded, the test chamber was evacuated and the capsule was removed. The passing criterion for the targets was a detected helium leakage rate equal to or less than 10^{-7} std cc/sec. All of the targets passed the leak test.

www.manaraa.com

3.2.2 Hydrostatic Pressure Test

A hydrostatic pressure test was performed in order to simulate the conditions the aluminum capsules would be subjected to in the nuclear reactor (HFIR). Up to two aluminum targets were inserted into a pressure chamber that was partially filled with approximately one liter of water. The remaining volume was filled with water and the cylindrical chamber was sealed. The chamber was pressurized to 1100 psi. Pressure was slowly released by opening and closing the bleed-off valve three times for less than one-half second each time. The pressure was maintained at 1100 psi for fifteen minutes. The chamber was depressurized and the target capsules were removed.

The capsules were placed in the laboratory oven for one hour at 220° Celsius, then removed from the oven and allowed to cool to room temperature. The capsules were individually weighed and recorded to the nearest milligram. If the weight had increased more than 3 milligrams or decreased more than 10 milligrams, the capsule would have been rejected.

3.3 Irradiation of the Neodymium Targets

All of the targets were irradiated at the hydraulic tube facility contained in the High Flux Isotope Reactor (HFIR). HFIR is an experimental research reactor located on the campus of ORNL. The 85 MW flux-trap type reactor, the most intense reactor based source of

www.manaraa.com

neutrons in the United States, generates a maximum neutron flux density of $2x10^{15}$ neutrons per square centimeter per second [15].

The hydraulic tube facility consists of a series of piping and instrumentation to shuttle a set of 2-inch long aluminum capsules between the flux trap and the capsule loading station while the reactor is in operation. The loading station is located in one of the storage pools adjacent to the reactor vessel pool. The Hydraulic Tube is located in position B3 of Figure 3.3 [15, 17].

The construction hydraulic tube facility allows for irradiation experiments ranging from as little as one minute to as long as 22 days (the maximum operating time). The facility can accommodate nine capsules, vertically stacked on top of one another in a 500-mm column.

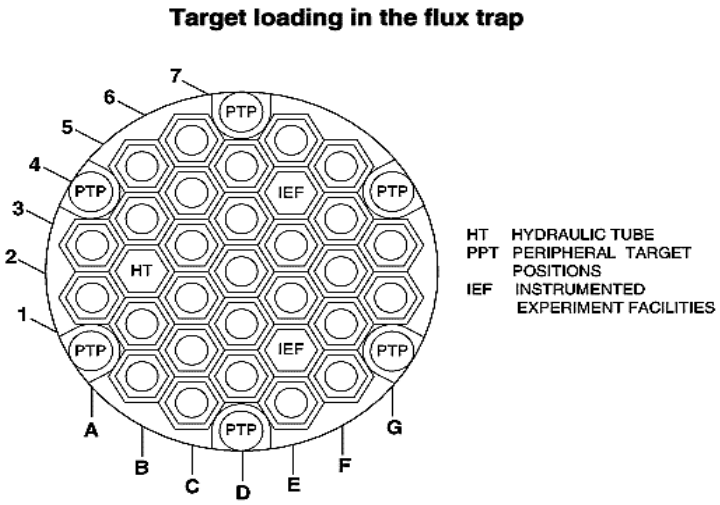

Figure 3.3: Schematic of the HFIR Flux Trap

www.manaraa.com

Position HT-1 is at the bottom, level with the bottom of the reactor core, while position HT-9 is at the top of the column, level with the top of the core. HT-5 is the position at the center line of the core [15]. This centerline position was desirable for these experiments but was not always available, so the position nearest to it was chosen. The loading and unloading of the capsules occurs during reactor operation by controlling the directional flow of cooling water through the tube.

3.3.1 Irradiation Schedule

Based on the desired resulting activity of 3.7×10^9 disintegrations per second (dps), which is equivalent to 100 mCi, the following equation was used to calculate the minimum time required in the reactor:

$$A = N\sigma\phi(1 - e^{-\lambda t_{ir}}) \tag{3.1}$$

Where A = radioactivity = 3.7×10^9 dps = 100 mCi

$$\text{N = number of atoms in target} = \frac{mass * A_v}{M} = \frac{0.004 grams * 6.023e23 atoms/mole}{146 grams/mole}$$

σ = neutron cross section of Nd-146 = 1.3 barns

Φ = neutron flux of reactor = 1.0×10^{15} n cm^{-2} s^{-1}

$$\lambda = \frac{\ln 2}{t_{1/2}} = \frac{\ln 2}{10.98 d}$$

t_{ir} = irradiation time

www.manaraa.com

Table 3.3: Irradiation Schedules for Targets

Target ID	End of Bombardment (EOB)	Irradiation Time	Target HT Position
NM-668	7/13/2009	96 hours	HT #3
NM-765	11/6/2009	96 hours	HT #5

The calculation above resulted in the minimum time required in the reactor to be 72 hours in order to achieve an activity of 3.7 x10^9 dps or 100 mCi. Based on this calculation, all three targets were irradiated between three and four days.

These targets were irradiated in positions HT-3 and -5 according to the schedule given in Table 3.3. The end of bombardment (EOB) indicates the day the targets were removed from the reactor. All targets were irradiated at the full reactor power of 85 MW.

3.4 Analysis of the Neodymium Targets

Following the irradiation, the targets were removed and transported to the hot cell where they were cut open to be analyzed. The targets were transported from HFIR anywhere from 25 to 75 days from the end of their irradiation cycles in the reactor. In order to be removed from the hot cell for further processing, the targets had to read at or below one Rem/hour. This usually did not occur, on average, until approximately fifty days from the end of bombardment (EOB). The high radioactivity from the targets was primarily due to the high activity from the quartz ampoules that masked the activity of the

www.manaraa.com

neodymium product. Twenty-seven days from the EOB of NM-668, the contact dose was 1.5 Rem/hr.

The daughter product remained in the oxide form, as promethium oxide (Pm_2O_3), despite the irradiation of the neodymium oxide target material. The oxygen atoms are not activated in the reactor since the neutron capture cross section of oxygen is so small.

Once the targets were removed from the hot cell, they were prepared for gamma spectroscopy analysis by one of two techniques:

- Technique I: Quartz ampoule was cut open and the irradiated material was dissolved in nitric acid. A small aliquot of the sample was analyzed (see Figure 3.4).
- Technique II: Quartz ampoule was placed on a card and analyzed, with no chemical dissolution (see Figure 3.5).

More details of these techniques are provided in the sections below.

3.4.1 Analysis Preparation Technique I

Target NM-668 was inserted into a glovebox and cut open along the equator using a glass cutter. The sample was dissolved in 0.5mL of 10M HCl and three drops of 8M HNO_3.

www.manaraa.com

Figure 3.4: Aliquot of Sample NM-668

The liquid sample was then collected in a glass container and set on a hot plate for approximately 45 minutes set at a low temperature. Once the liquid was evaporated, one milliliter of 0.1M HCl was added to the specimen. Using a calibrated pipette, 100-microliters, or 10% of the total sample size, were extracted into a plastic cylinder for analysis as seen in Figure 3.4.

3.4.2 Analysis Preparation Technique II

Target NM-765 was removed from the hot cell and transferred to a laboratory where it was placed under a hood. The target contained two ampoules wrapped in aluminum foil.

www.manaraa.com

Figure 3.5: Sample NM-765T

Each ampoule was removed, carefully marked, and positioned in the center of a place card with a piece of clear tape over top of the ampoule to hold it in place as seen in Figure 3.5. The card then can be inserted directly into the sleeves of the shelf inside the gamma spectrometer.

3.4.3 Radioactivity Measurement

The radioactivity of the samples involved in this project was measured using Gamma-ray Spectrometry. The spectrometer consists of a calibrated high purity Germanium (Ge) source detector, a spectroscopy amplifier, an analog-to-digital converter (ADC), and a PC-based multi-channel analyzer interface. The ADC has 4096 channels that sort the gamma photons according to their energies. The detector has a resolution of 1.0 keV at 123 keV and 1.8 keV at 1332 keV [17]. Efficiency and energy calibrations were

www.manaraa.com

determined with gamma-ray sources traceable to the National Institute of Standards and Technology (NIST). The efficiency calculations were factored into the resulting data analysis.

The samples were counted with dead times of the analyzer not exceeding 10% between 1 cm and 25 cm distances from the surface of the Ge detector. The radioactivity (counts per second) was converted to absolute disintegrations per second (A^0, dps) using appropriate corrections for the gamma-ray intensity and detector efficiency. A europium-152, -154 & -155 certified standard was used to generate the efficiency curves seen in Figure 3.6 for the gamma spectrometer used in the analysis of the samples.

The counts were made at different shelf levels as the radioactivity of the sample decreased. The final count to calculate the impurities in sample NM-668 was set on the 1-cm shelf; however, the final count to calculate the product yields of Nd-147/Pm-147 product was set on the 5-cm shelf. The reason for this is in order to minimize the error in calculating the product yields. Counting the sample on the 1-cm shelf, or essentially on the source, allows for a much wider angle of inflection of the photons and vastly increases the uncertainties in the measurements. The impurities represented such a small percentage of the overall activity of the material that even a large uncertainty will not grossly affect the final results. The results of the uncertainty analysis are discussed in section 4.3. Moving the sample up, even at 5-cm, allows for the consideration of the sample as a point source, thus minimizing the error in the yield calculations. NM-755T

www.manaraa.com

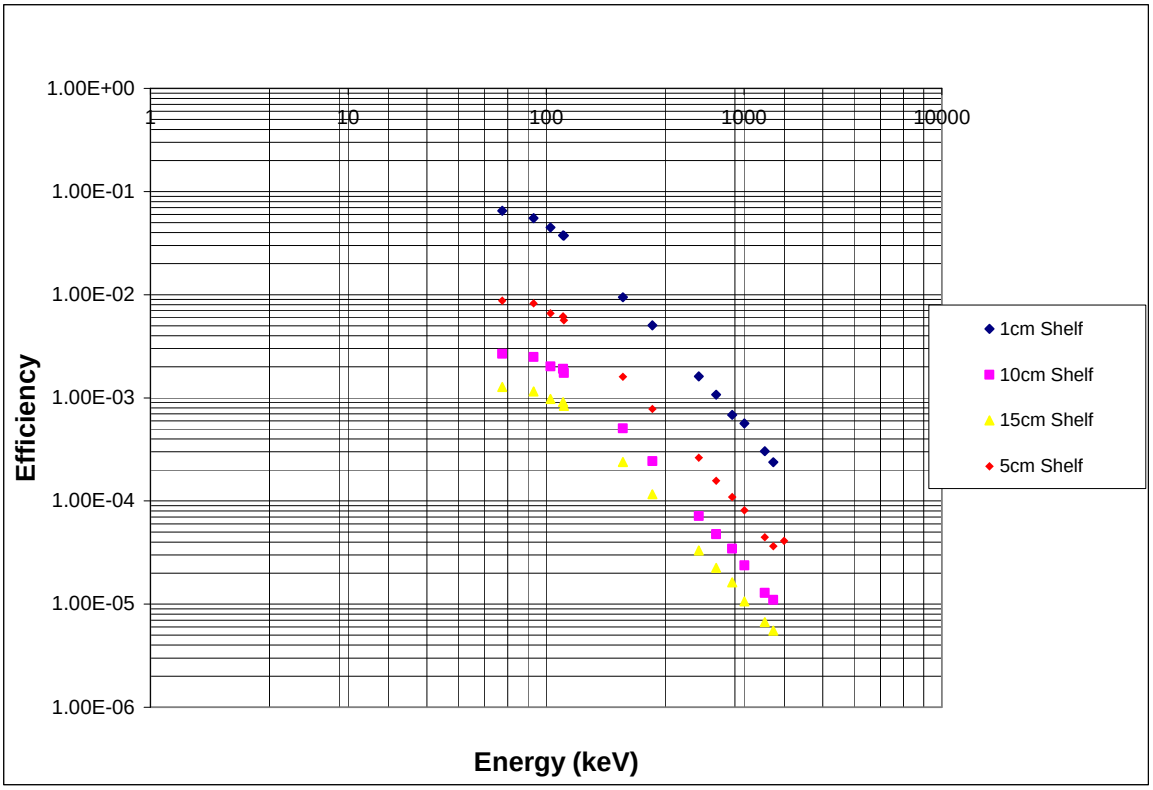

Figure 3.6: Gamma Spectrometer Efficiency Curves

and -755B were counted on the 10-cm shelf for both the impurities and the product yield final counts due to the high radioactivity of the samples.

www.manaraa.com

CHAPTER 4

RESULTS

4.1 Gamma Energy Spectrum

Each sample was counted individually for different periods of time and from various distances from the gamma spectrometer source. The gamma spectrometer had six shelves ranging from one to twenty-five centimeters from the source. NM-668 was counted for the longest period of time – at least once a week for twenty-five weeks. The other two samples, NM-765T and -765B, were counted for approximately ten weeks.

The results of the gamma energy spectrum were taken directly from the output program files of the gamma spectrometer and the energies were plotted against the counts (disintegrations). The *Atomic Data and Nuclear Data Tables* [18] were used to identify each photon energy peak listed on the gamma spectrometer printouts. Figure 4.1 shows the number of counts as a function of energy for target NM-668 eighty-one days after the end of bombardment (EOB). In order to view the remainder of the peaks in more detail, the gamma energies were plotted against the log of the counts, as seen in Figures 4.2 and 4.13.

www.manaraa.com

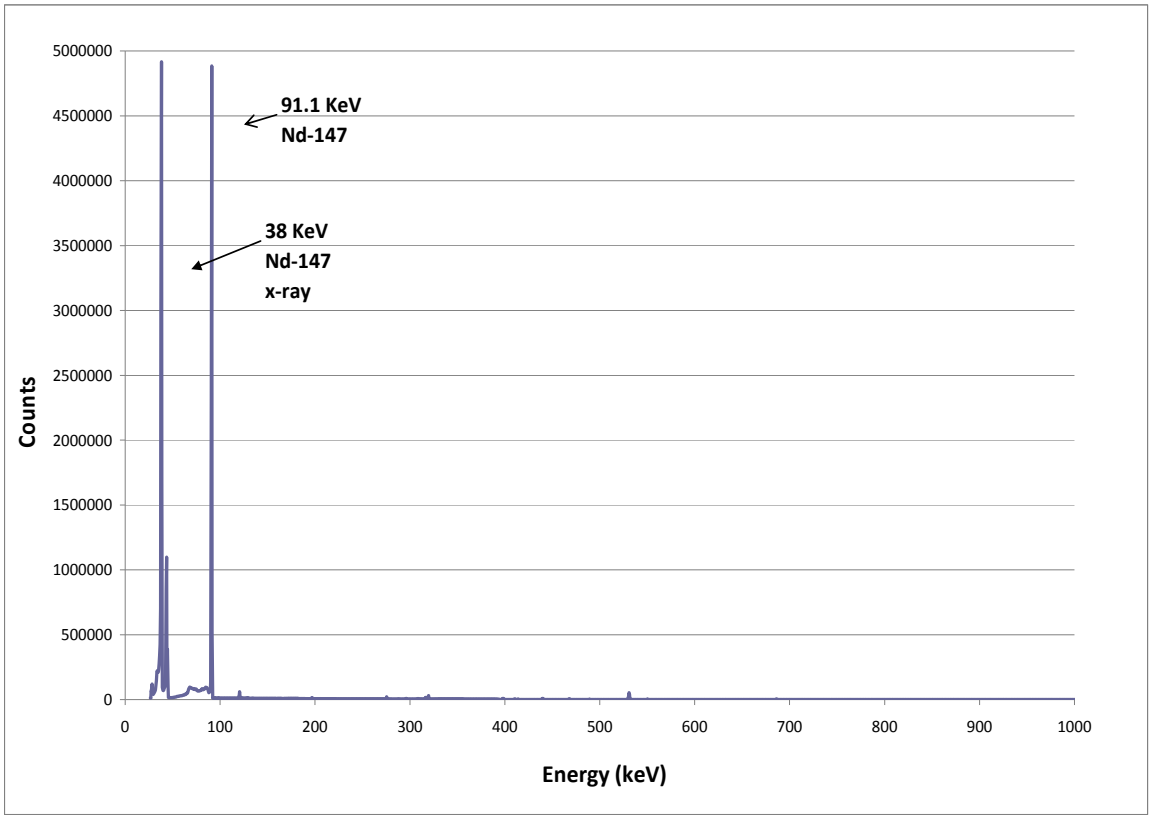

Figure 4.1: Gamma Spectrum of NM-668 – 81 days from EOB;
Count time = 2 hours on 20cm shelf

www.manaraa.com

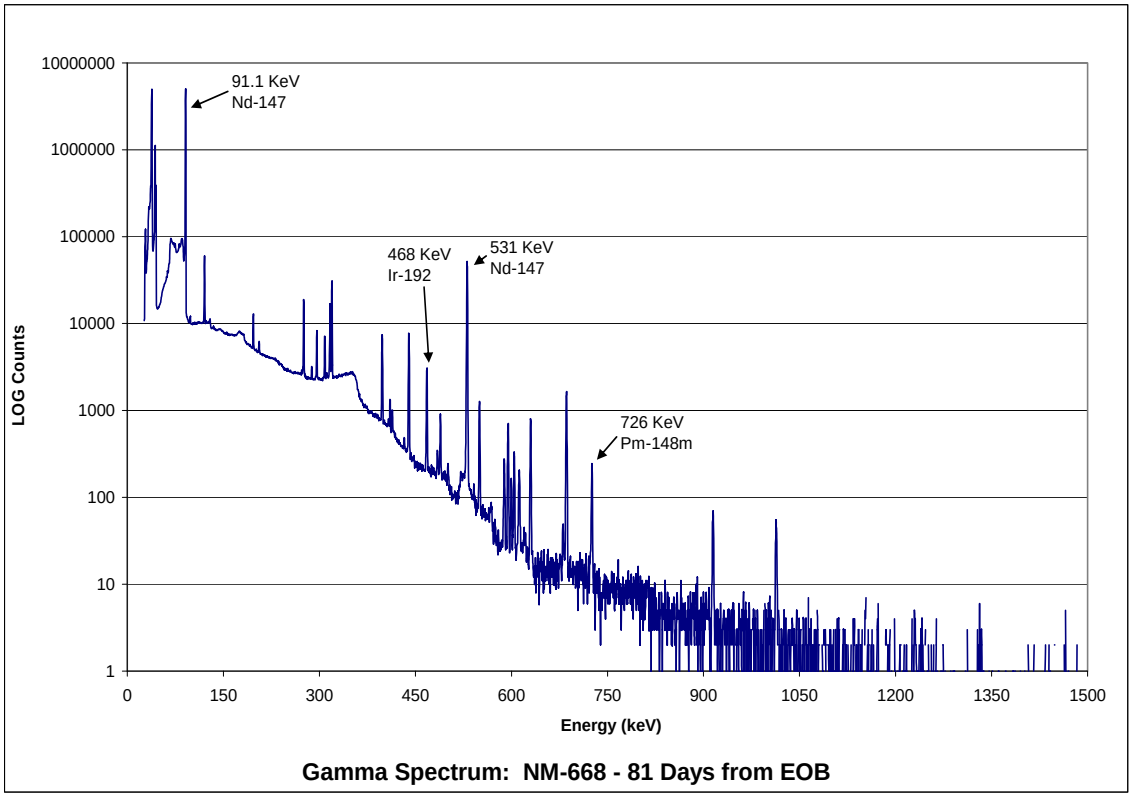

Figure 4.2: LOG Plot of Gamma Spectrum: NM-668 - 81 Days from EOB

www.manaraa.com

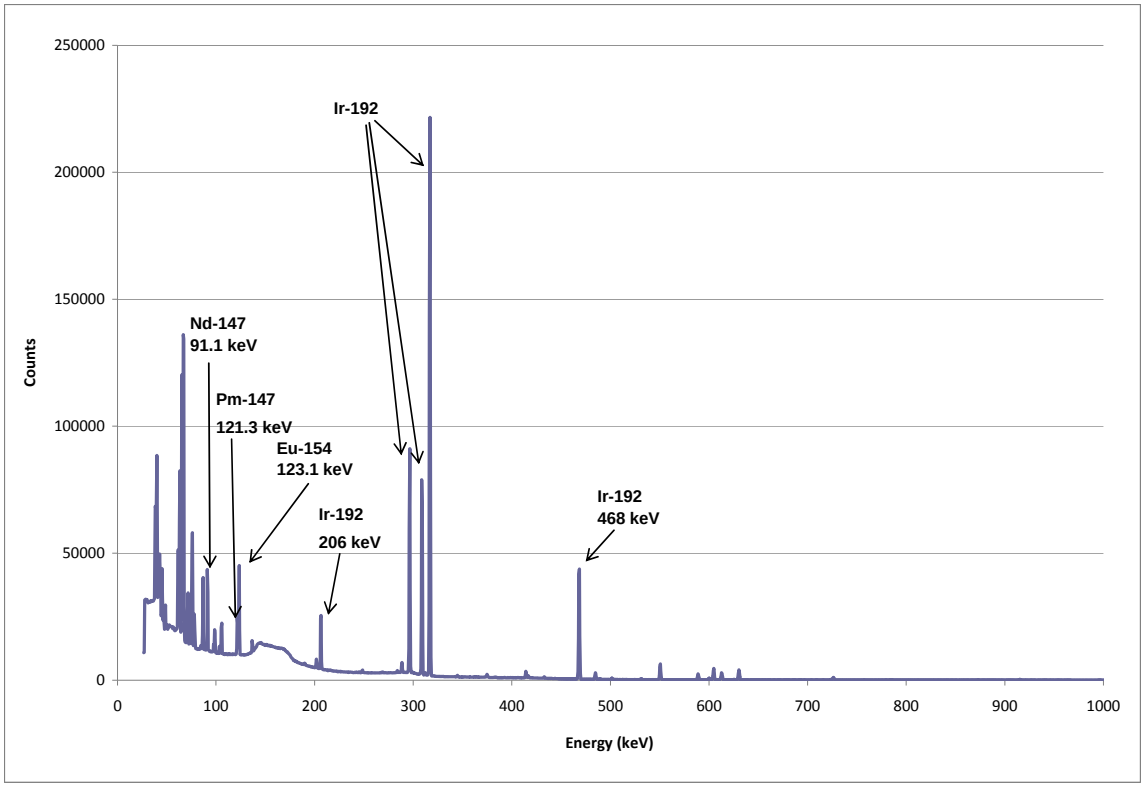

Figure 4.3: Gamma Spectrum of NM-668 - 211 days from EOB (Compare to Figure 4.1)

4.1.1 Analysis of Radionuclide Impurities

The 4096-channel analyzer gamma spectrum was sectioned into multiple plots to view the details of the energy peaks on different scales. This allowed for better resolution and identification of the isotopic impurities. Eight plots were generated for each of the three samples analyzed. Figures 4.4 through 4.11 show the gamma energy spectrums for sample NM-668. Figures 4.12 through 4.28 show the spectrums for samples NM-765T and -765B.

www.manaraa.com

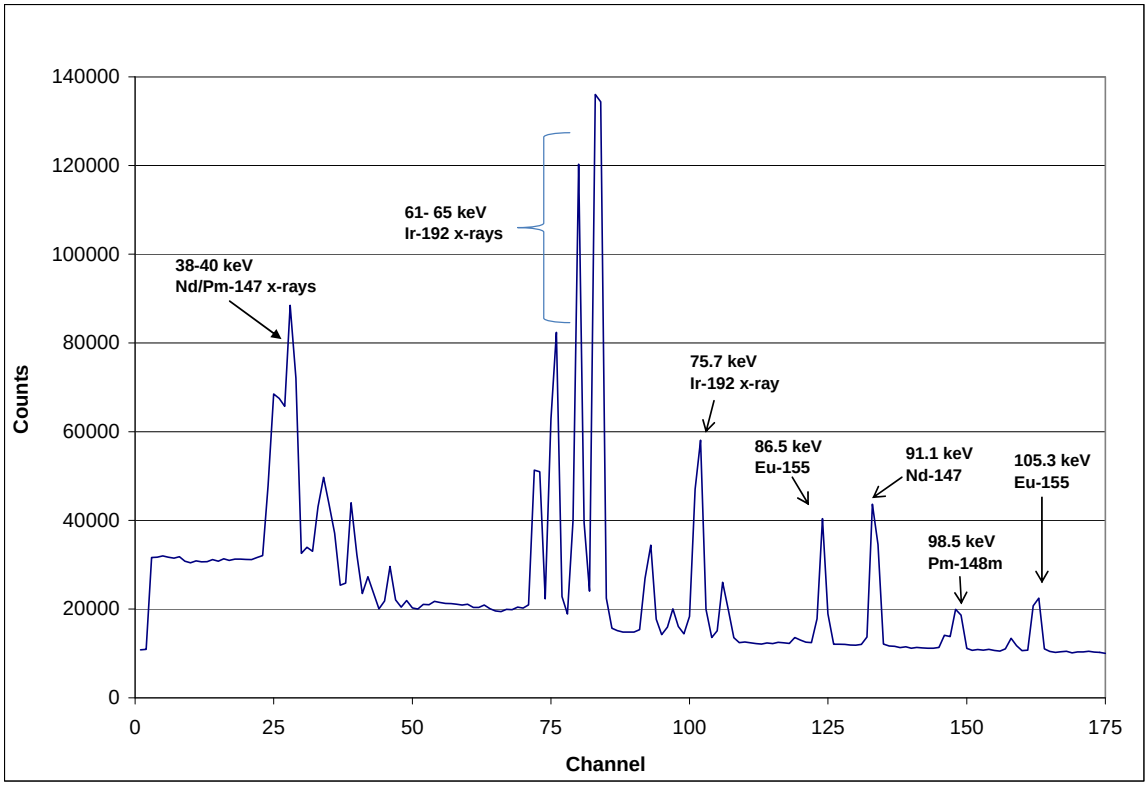

Figure 4.4: Gamma Spectrum of NM-668 – Channel 0-175

www.manaraa.com

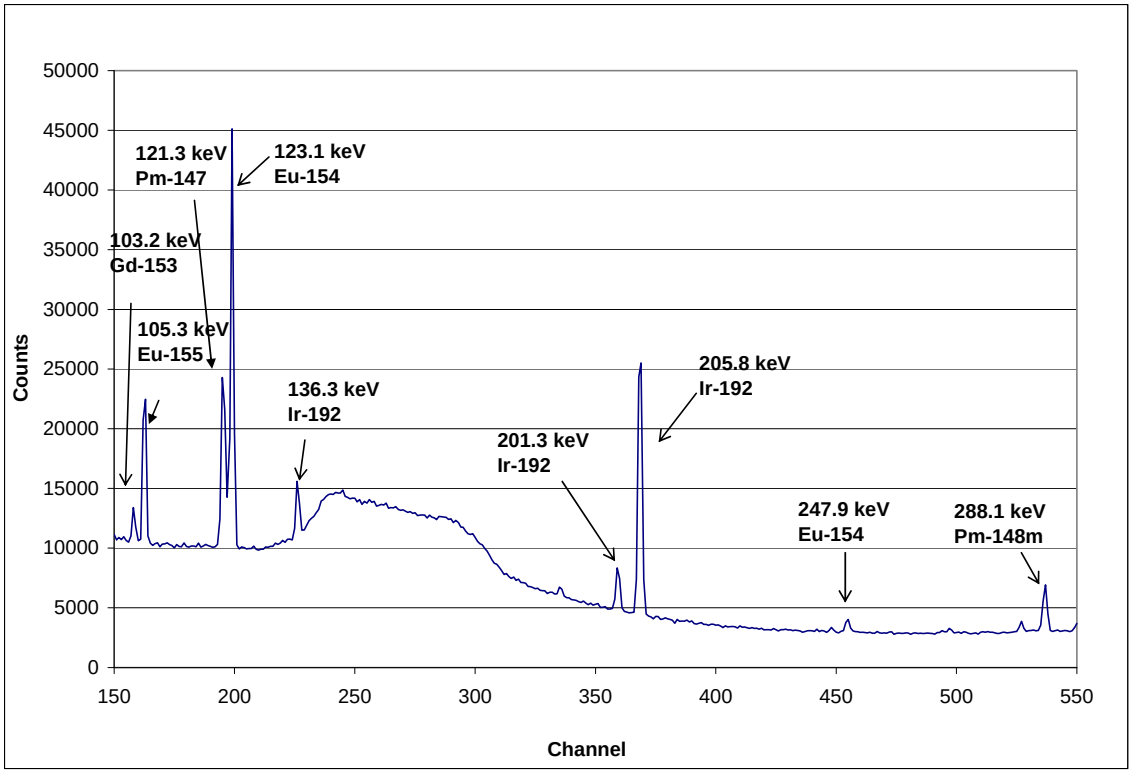

Figure 4.5: Gamma Spectrum of NM-668 – Channel 150-550

www.manaraa.com

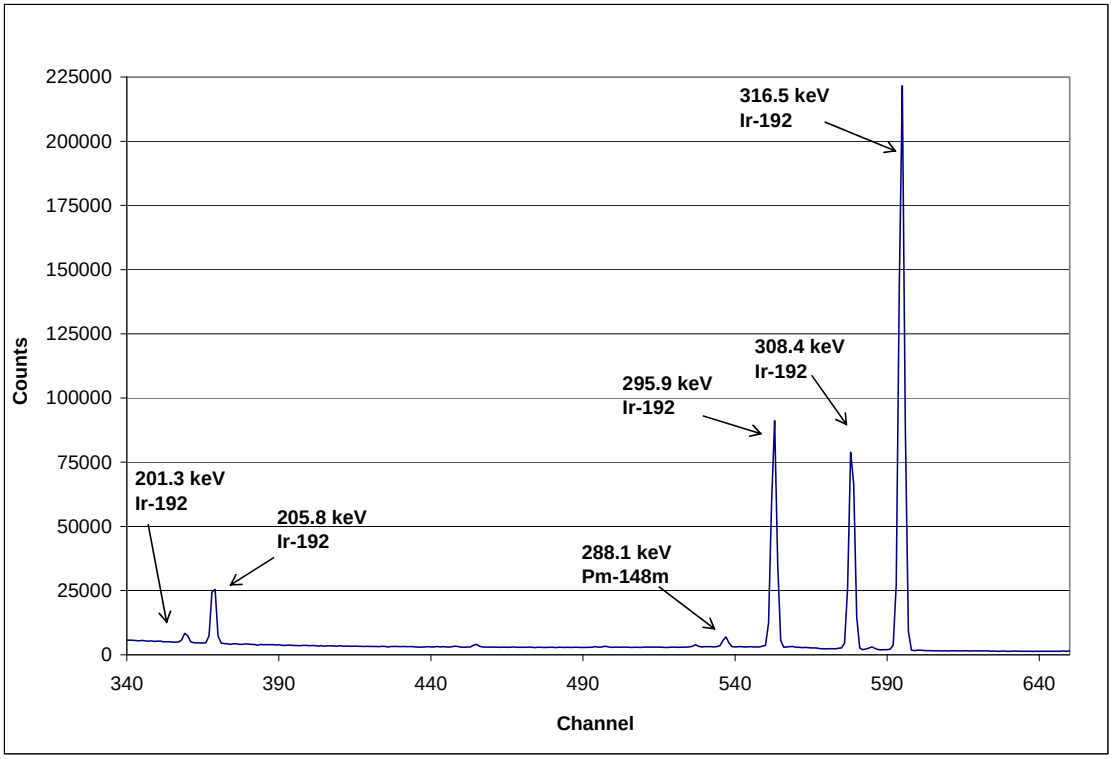

Figure 4.6: Gamma Spectrum of NM-668 – Channel 340-650

www.manaraa.com

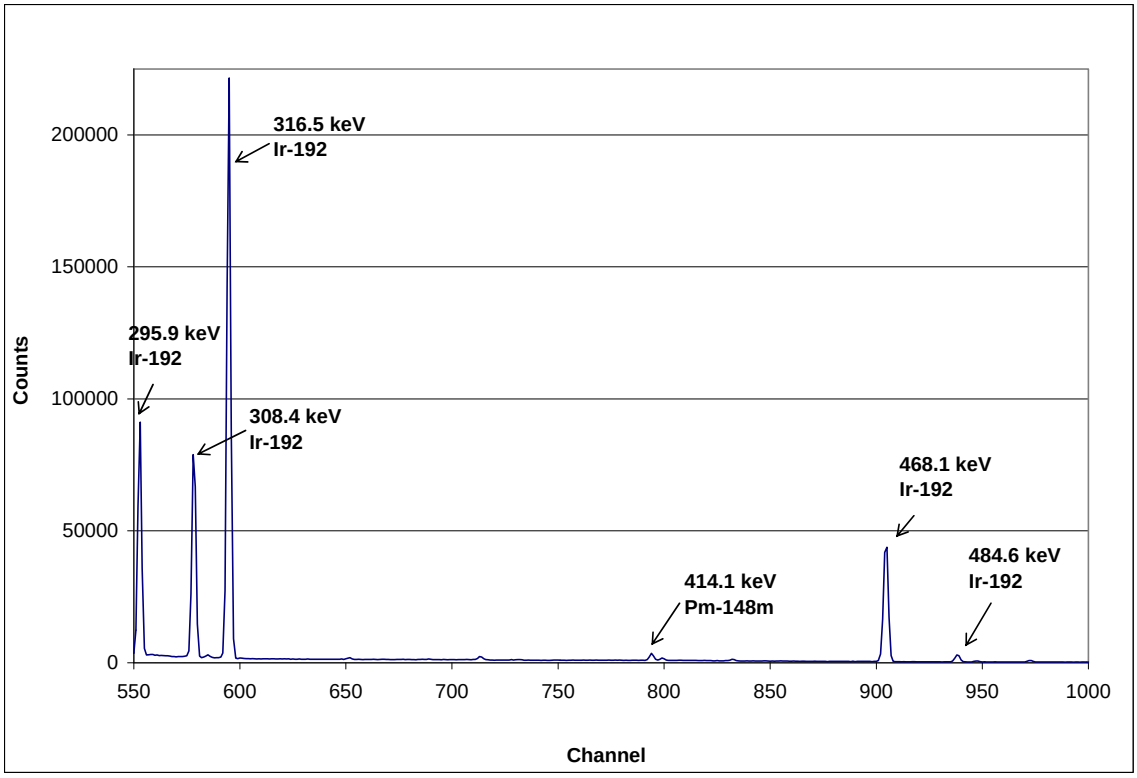

Figure 4.7: Gamma Spectrum of NM-668 – Channel 550-1000

www.manaraa.com

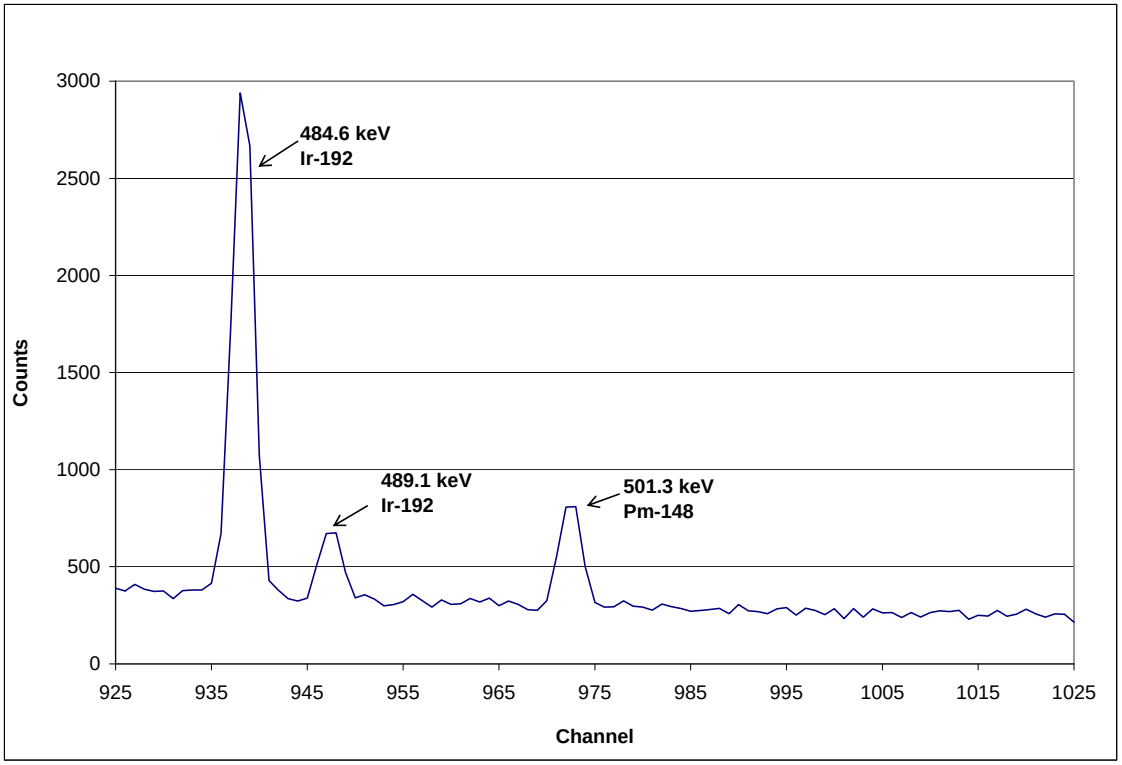

Figure 4.8: Gamma Spectrum of NM-668 – Channel 925-1025

www.manaraa.com

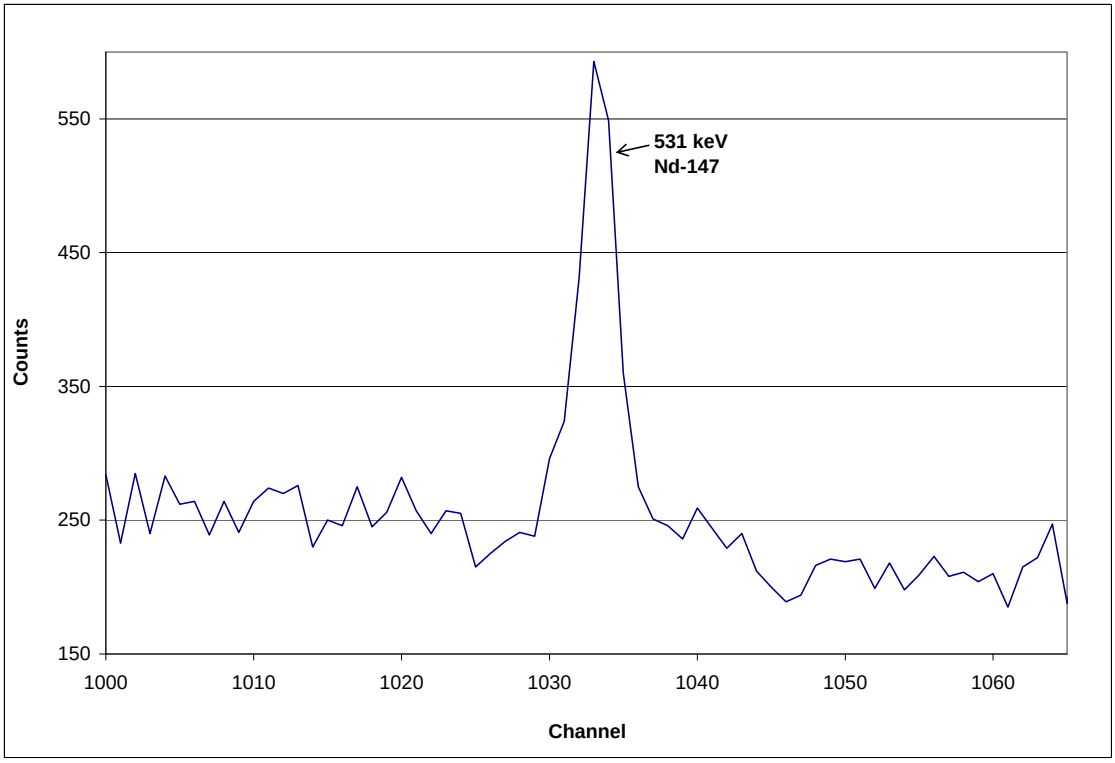

Figure 4.9: Gamma Spectrum of NM-668 – Channel 1000-1070

www.manaraa.com

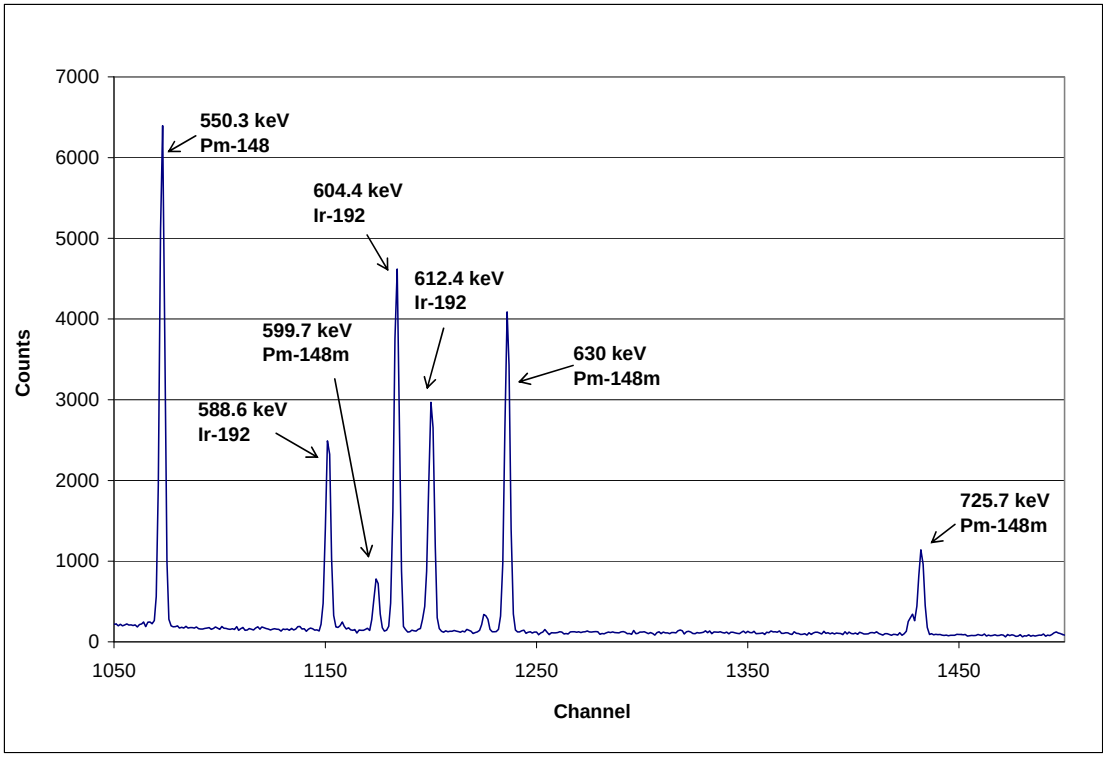

Figure 4.10: Gamma Spectrum of NM-668 – Channel 1050-1500

www.manaraa.com

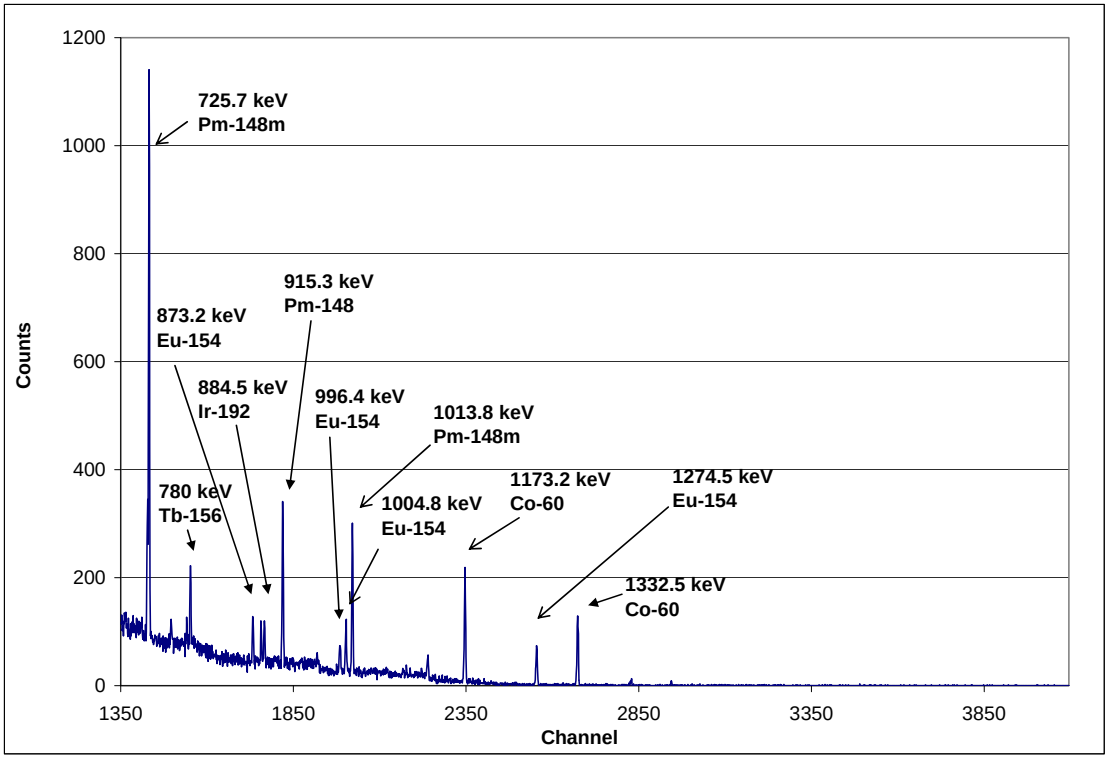

Figure 4.11: Gamma Spectrum of NM-668 – Channel 1350-4097

4.1.2 Calculation of the Radioactivity

The peak analysis reports from each run provided the counts per second used to calculate the radioactivity, expressed as specific activity, for each isotope. Table 4.1 shows the gamma peak used to calculate the radioactivity. The intensities (%) of the gamma photons were taken from the published values in volume 29 of the "Atomic Data and Nuclear Data Tables" [19]. In order to account for the efficiency of the detector and the intensity of the gamma photons, a conversion factor was applied to the calculation of the radioactivity.

www.manaraa.com

$$\text{Conversion Factor} = C_F = \frac{I}{100} \times E_S \times 3.7x10^4 \quad (\mu Ci^{-1}) \qquad (4.1)$$

Where: I = Intensity of photon (%)

E_S = Detector Efficiency for γ-ray (using Figure 3.6)

1 μCi = $3.7x10^4$ μBq

The detector efficiency combines both the intrinsic efficiency and the geometric efficiency, i.e. – the distance between the detector and the source. The radioactivity in micro-Curie per milligram for each isotope was calculated using the following equation:

$$R = \frac{CPS}{C_F} \times D_f \times \frac{1}{M_{Nd-146}} \quad (\mu Ci/mg) \qquad (4.2)$$

Where: CPS = counts per second of photon peak

D_f = dilution factor (only used for NM-668)

$M_{Nd\text{-}146}$ = mass (mg) of Nd-146 (calculated using equation 3.1)

In order to calculate the radioactivity of the isotopes contained in sample NM-668, a dilution factor of ten had to be applied since only a 10% aliquot of the sample was analyzed (see section 3.4). The other two samples were analyzed in solid form.

www.manaraa.com

TABLE 4.1: Summary of Impurities at EOB

		Radioactivity (μCi/mg of Nd-146 target) at EOB		
Radioisotope	**Half-Life**	**NM-668**	**NM-765T**	**NM-765B**
Pm-148	41.3 d	3.07E+01 ±1.6E+01	2.46E+02±3.1E+01	3.60E+02±1.1E+02
Eu-152	13.3 y	6.64E+00±6.2E-01	nd	nd
Eu-154	8.8 y	2.42E+01±1.8E+00	8.82E+00±1.3E+00	1.25E+01±2.0E-01
Eu-155	4.68 y	7.38E+00±1.6E+00	4.57E-01±4.0E-01	7.10E-01±5.8E-01
Gd-153	247 d	2.51E+00±1.6E-01	5.78E-01±4.9E-02	1.34E+00±1.3E-01
Ir-192	78.8 d	5.08E+02±1.4E+02	8.97E-01±5.9E-02	2.61E+00±1.1E-02
Co-60	5.27 y	1.38E+01±2.4E+00	6.07E+01±5.2E+01	1.86E+00±2.9E-02
Sc-46	84 d	2.31E+00±1.6E-01	2.42E+02±2.6E+01	3.62E+02±2.8E+01
Tb-160	72d	nd	2.79E+01±1.0E+01	3.30E+01±6.9E-01
Ce-141	32.5 d	nd	8.76E+00±1.3E+00	1.27E+01±7.4E-01

4.1.3 Summary of Impurities

Table 4.1 shows a summary of the impurities for each sample as well as a calculation of the radioactivity, with errors, for each isotope. A total of ten different isotopes were identified in the three samples analyzed. The radioactivity of each isotope was calculated for the activity at the EOB. If the isotope was not detected in the analysis, it was indicated in Table 4.1 as "nd."

4.1.4 Promethium-147 Product Yield

The theoretical yield of Pm-147 was calculated for each sample using equation 3.1 and compared to that of the experimental yield calculation using equation 4.2. The experimental yield of Pm-147 for sample NM-668 was 765 micro-Curies per milligram

www.manaraa.com

(μCi/mg) while the theoretical yield was 611 μCi/mg. These values were calculated and measured approximately 240 days from the EOB.

4.2 Shielding Recommendation

An estimate of the required lead shielding was calculated using equation 2.14 from the published variables and coefficients (i.e.- buildup factors) [14, 29]. Due to complexity of the calculation, an iterative process was used to calculate the required thickness of the shielding. Lead was chosen as the shielding material due to its high attenuation and the desire to contain the possible device in a small area. The shielding was only calculated for sample NM-668 (97.5% Nd-146), using the radioactivity calculations provided in Table 4.5 (~240 days from EOB), since it demonstrated the best overall Pm-147 product yield and would be more likely to be chosen over the other two samples.

It was estimated from the literature that a useful amount of Pm-147 for application as a low power source would be between 1 and 100 curies. The total activity (product and impurities) of sample NM-668 was 767 μCi/mg or 0.767 Ci/g as seen in Table 4.5. Thus, the shielding calculations were based on 76.7-Ci source or ~100 grams of Pm-147 in order to simplify the calculations. The dose rate from all the measured energies of the five isotopes was averaged to provide the final calculated dose rate. Table 4.7 contains all the parameters for the calculation. The following assumptions were made for the calculation:

www.manaraa.com

- Point isotropic source.
- Soft tissue can be reasonably simulated by water (use mass energy coefficient for water).
- The source will contain the same specific activities as NM-668 at ~240 days from EOB.
- Co-60, Ir-192, and Sc-46 will be removed by ion exchange methods and will not contribute to the dose.
- The gamma emission from Pm-147 is negligible.
- Pm-146 is present in the sample and will contribute to the dose. The activity of it is equal to the limit of detection calculated in section 4.3.

The dose rates were calculated at the surface of the lead shielding meaning that the distance from the point source was equal to the lead shielding thickness. These parameters were chosen to simulate the worst case scenario of handling a device such as a beta-battery. The calculated results are contained in Table 4.6, while Figure 4.12 shows a graphical representation of the results.

www.manaraa.com

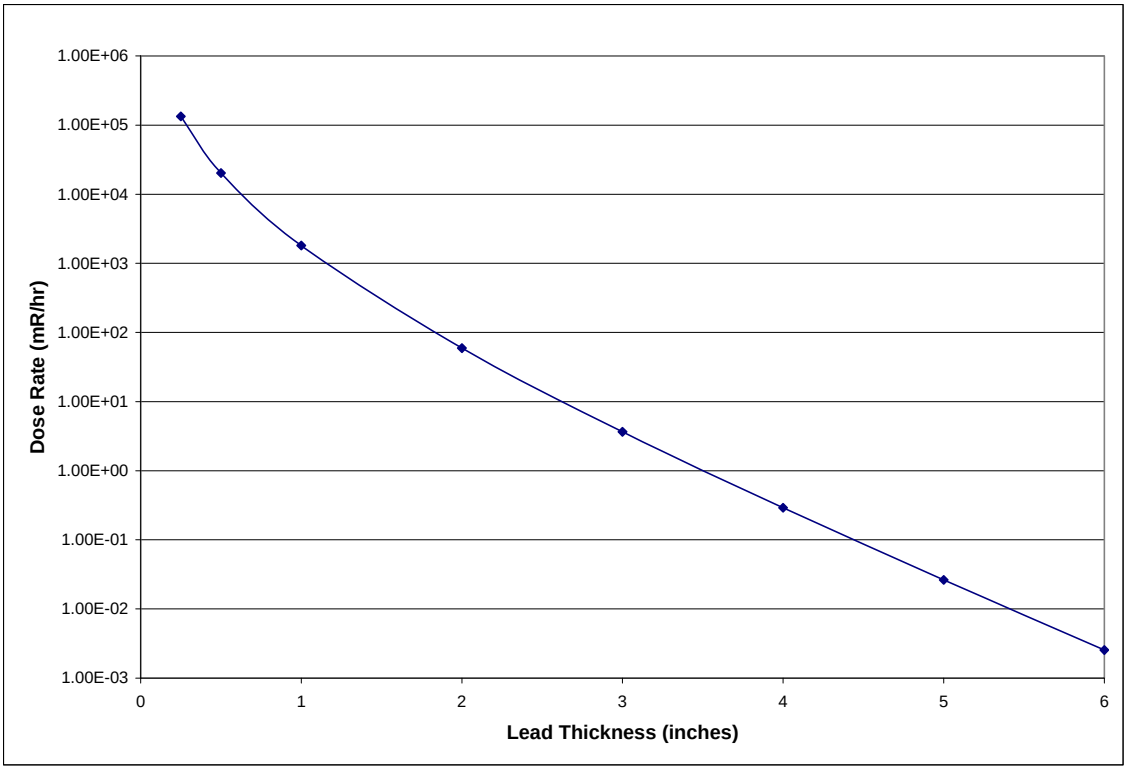

Figure 4.12: Dose Rates of Lead Shielding for NM-668

A thin plastic liner (~5mm) around the source will be required to shield against the bremsstrahlung radiation caused by the high energy beta particles. This is not taken into account for the calculation of the lead shielding required for γ-rays due to its minimal thickness; however, it is still required.

The International Commission on Radiological Protection (ICRP) recommends a maximum annual dose of 2,000mrem [28]. In following this recommendation, it was estimated the dose rate of a device using the 76.7Ci Pm-147 source would be required to stay at or below 1 mR/hr; thus, requiring at least a 3.5-inch lead shield to protect a human while using such a device within close contact to the body. This calculation serves only

www.manaraa.com

as an estimate. More detailed analysis would be required to provide increased certainty of the shielding requirements.

4.3 Uncertainty Analysis

A number of different techniques were analyzed to determine the uncertainty of the measured impurities. One simple method would be to use the counting errors for the gamma photon peaks directly from the program file of the gamma spectrometer following a sample count as seen in Table 4.2. These values represent system counting errors as calculated by the computer software. Samples were counted for long durations such that these counting errors were below five percent.

In order to capture a better overall uncertainty of the measured values, a separate technique was exercised to calculate the deviation of the activity at a given instance of time. Equation 4.4 provided an estimate of the overall uncertainty of the measured radioactivity at each isotope gamma energy peak.

www.manaraa.com

TABLE 4.2: Error Percentages on Analyzed Gamma Peaks

Radioisotope	Gamma Energy Peak Used in Counting (keV)	NM-668 % Error	NM-765T % Error	NM-765B % Error
Nd-147	91.1	1.16	0.07	0.06
Pm-147	121.3	0.36	nd	nd
Pm-148	550	0.72	0.53	0.44
Eu-152	344	4.95	nd	nd
Eu-154	123.1	0.23	0.68	0.58
Eu-155	105.3	1.67	0.7	0.41
Gd-153	103.2	1.92	5.23	2.13
Ir-192	316	0.08	6.64	3.02
Co-60	1173	1.89	1.03	9.26
Sc-46	1120.5	8.01	0.58	0.48
Tb-160	298.6	nd	5.8	2.36
Ce-141	145	nd	1.95	1.67

First, the activity at the EOB, A_0, must be reverse calculated for each isotope using the counts per second from the gamma spectra analysis at different times. Since the radioactivity at time, n, is calculated using equation 4.2 from the given counts per second, the activity at the EOB for each isotope can be calculated using equation 4.3. This calculation is completed at different times according to the number of data analyses that were run on the sample.

$$A_0 = A_n e^{\lambda t_n} \tag{4.3}$$

Where: A_0 = activity at the EOB

A_n = calculation of the radioactivity at time n using equation 4.2

λ = decay constant

www.manaraa.com

t_n = # of days from the EOB

$$\sigma = \sum \frac{\left|\overline{A}^0 - A_n^0\right|}{N} \qquad (4.4)$$

Where: $\overline{A}^0 = \frac{A_1 + A_2 + \ldots + A_N}{N}$ = mean activity at the EOB

A_n^0 = activity of sample n at the EOB

N = # of samples

Table 4.3 shows the total error results for each sample as calculated using equation 4.4. These values were reported with the summary of the impurities in Table 4.1.

TABLE 4.3: Total Error for the Analyzed Gamma Peaks

Radioisotope	Gamma Energy Peak Used in Counting (keV)	NM-668 % Error	NM-765T % Error	NM-765B % Error
Nd-147	91.1	31.6	6.0	38.6
Pm-147	121.3	7.3	nd	nd
Pm-148	550	52.5	12.8	29.9
Eu-152	344	9.4	nd	nd
Eu-154	123.1	7.8	14.6	1.6
Eu-155	105.3	21.5	87.9	82.4
Gd-153	103.2	6.6	8.6	9.5
Ir-192	316	28.2	6.6	0.4
Co-60	1173	17.3	8.6	1.6
Sc-46	1120.5	6.9	11	7.7
Tb-160	298.6	nd	37.3	2.1
Ce-141	145	nd	15.4	5.8

www.manaraa.com

4.3.1 Limit of Detection for Pm-146 Impurity

The presence of fast neutrons (> 2MeV) in the flux trap of the HFIR induces the following (n,2n) reaction [10]:

$$Pm^{147} + n \rightarrow Pm^{146} + 2n$$

Pm-146 ($t_{1/2}$ = 5.5y) is an undesirable impurity of the Pm-147 product since it has a long half-life and emits three high energy γ-rays including at 453keV that has a 65% probability of occurrence. Similar to Pm-148, it is difficult to remove.

Using the most abundant gamma energy peak for promethium-146 (Pm-146) at 453keV, the limit of detection can be calculated. The gamma spectrometer has a limit of detection – that is the limit in activity at which the counting device cannot detect a known photon peak. The intensity of the photon that is not seen by the detector at 453keV in counts or disintegrations per unit time will result in the limit of detection. Using the NM-668 gamma spectrum analyzed 211 days from the end of bombardment; the counts at each channel within plus or minus 5keV of the 453keV peak were summed to determine the average number of counts within the 18-channel range. It was important to choose an area on the spectrum where there were no energy peaks. As seen in Figure 4.7, there were no energy peaks between channels analyzed – from channel 855 to 872. In equation 4.4 the average number of counts per channel is multiplied by four since a gamma peak is typically composed of four channels (i.e.- ~0.5keV/channel).

www.manaraa.com

In order for a photon peak to be visible, the count rate under the photon peak must be larger than the sum of the background count (B) and the background error (σ_B):

$$LOD = B + \sigma_B - B = \sigma_B \tag{4.5}$$

Where $B = \dfrac{4(channels) \times \dfrac{TotalCounts}{total\#channels}}{runtime} = \dfrac{4 \times \dfrac{9648counts}{18channels}}{180\,\text{min}}$ (counts/min)

$$\sigma_B = \sqrt{CPM} = \sqrt{\frac{4 \times \frac{9648}{18}}{180\,\text{min}}}$$

The limit of detection was calculated to be 2.06×10^{-1} counts per second. When the conversion factor is applied to calculate the radioactivity using equations 4.1 and 4.2, the resulting limit of detection of Pm-146 is 2.1 nCi/mg, meaning that under our experimental conditions levels of Pm-146 has to be below 2.1 nCi/mg; otherwise, any level larger than 2.1 nCi/mg would have been detected.

www.manaraa.com

CHAPTER 5

DISCUSSION OF RESULTS

5.1 Radioistopic Impurities

For all three samples the initial gamma spectrum (<90 days from EOB) was dominated by the 91.1 keV peak for neodymium-147 ($t_{1/2}$ = 11 days). The 91.1 keV peak was the most abundant (28%) neodymium-147 gamma photon peak. The 91 keV peak in figure 4.1 has a corresponding x-ray energy peak at 38 keV due to the interaction of the gamma photons with the outer shell electrons. A decrease in the activity of the Nd-147 following its beta decay to the Pm-147 product gave rise, and an opportunity to detect, the activity of the impurity isotopes such as europium-154 as seen in figure 4.1 – counted 211 days from the end of bombardment. Notice that the Nd-147 91.1keV peak decreased from nearly $1.0x10^7$ to less than $1.5x10^5$ counts in the 130 days between the analyses. Figure 5.1 shows the decrease in the specific activity (μCi/mg) of Nd-147 as measured by the gamma spectrometer at different times from the EOB.

www.manaraa.com

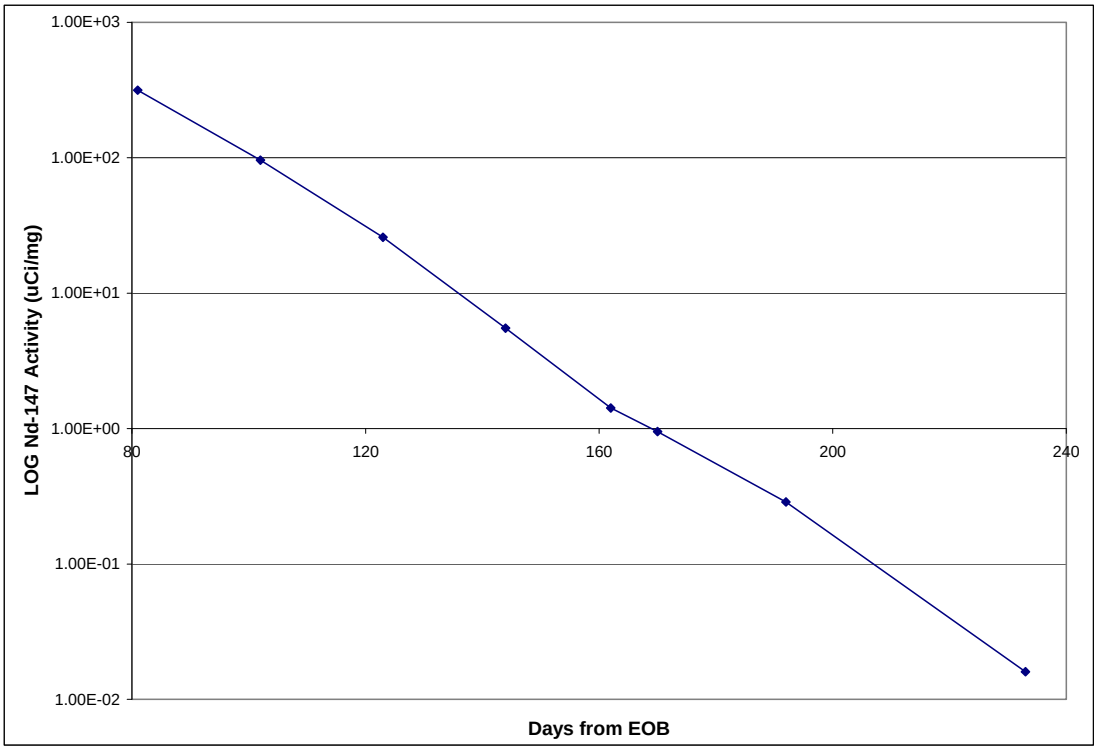

Figure 5.1: Sample NM-668 - Activity of Nd-147

Compton scattering along with secondary radiations, including Bremsstrahlung which is caused by interactions with the beta particles, accounted for the high background seen in the gamma spectra. The background values decreased over time with subsequent decay of Nd-147 to Pm-147 and allowed for the presence of other isotopes to be seen. In order to ensure all of the isotopes were seen on the gamma spectrum analysis, the final counts used in this analysis were not conducted until at least 110 days (or ~10 half-lives of Nd-147) from the end of bombardment. This ensured that at least 99.9% of Nd-147 had decayed to the daughter product, Pm-147.

www.manaraa.com

5.1.1 Concentration of the Impurities

The activity of each isotope was divided by the total measured activity to obtain the concentration for each radioisotope. Obviously, the higher enriched Nd-146 assay sample resulted in a noticeably higher product yield. As seen in Table 5.1, 99.7% of the activity from NM-668 (97.5% Nd-146) was attributed to the Nd-147/Pm-147 product while only 86% and 87% product activity yields were measured for NM-765T (86.8% Nd-146) and -765B (86.8% Nd-147), respectively.

The highest quantity impurity in sample NM-668 was Iridium-192 which only accounts for less than one percent of the total activity. It most likely originated from the tools used to prepare the Nd_2O_3 that contained traces of iridium metal. Promethium-148 was not a substantial contaminant in NM-668 but accounted for more than 5% of the sample activity in both NM-765T and -765B.

Samples NM-765T and -765B had a large proportion of Scandium-46 (Sc-46). Sc-46 is a single photon emitter with a half-life of 84 days. It is found in almost all the rare-earth elements including neodymium [24].

www.manaraa.com

Table 5.1: Concentration of Radioisotopes

Radionuclide	% of NM-668 Activity at 235d from EOB	% of NM-765T Activity at 128d from EOB	% of NM-765B Activity at 128d from EOB
Nd-147	2.09E-03	8.61E+01	8.74E+01
Pm-147	9.97E+01	nd	nd
Pm-148	1.62E-02	5.70E+00	5.74E+00
Eu-152	3.56E-03	0.00E+00	0.00E+00
Eu-154	1.30E-02	2.07E-01	2.02E-01
Eu-155	3.96E-03	1.07E-02	1.15E-02
Gd-153	1.34E-03	1.36E-02	2.16E-02
Ir-192	2.70E-01	2.09E-02	4.19E-02
Co-60	7.42E-03	1.43E+00	3.02E-02
Sc-46	1.23E-03	5.64E+00	5.82E+00
Tb-160	0.00E+00	6.50E-01	5.30E-01
Ce-141	0.00E+00	2.02E-01	2.02E-01

5.2 Pm-147 Yield

The quantification of Pm-147 was difficult since it only emits a few very low abundance gamma photons. The signature gamma energy peak for the identification of Pm-147 is at 121.3 keV; however, the abundance of that gamma energy peak is only 0.0028%. The decay and transmutation of Nd-147 was witnessed over the course of this analysis via the reduction in counts at the 120.5-keV and 91-keV peaks.

At approximately 150 days from the end of bombardment (EOB), equivalent to approximately thirteen half-lives of Nd-147, the activity of the 120.5-keV peak no longer appeared in the output of the analysis. When this peak disappeared, the 121.3-keV Pm-147 signature gamma began appearing in the spectrum. This 121.3-keV peak was always there but was masked by the high activity of the Nd-147 as seen in Figure 4.5. The

www.manaraa.com

121.3-keV peak was not detectable in two of the three samples – NM-765T and -765B since these two samples were analyzed less than 150 days from the EOB. The ratio of the experimental to theoretical Pm-147 yield was 1.25, which represents a close agreement between the two values.

5.3 Lead Shield Recommendation

The shielding estimates were provided with the assumption the Pm-147 would be used in such a manner that involves close human contact – on or near the human body for a large amount of time. Thus, the recommendation of 3.5-inches of lead shielding for a 76.7-Ci Pm-147 source reflects this assumption. Obviously, less shielding would be required for an application with little or no human contact.

Pm-148 and Eu-154 were the highest contributors to the dose. Both emit high energy and abundant γ-rays. Pm-146 ($t_{1/2}$=5.5y) was the next highest contributor and also would be a concern for shielding. These three radioisotopes are difficult to remove and shielding must be designed to limit their γ-rays.

5.4 Removal of Impurities and Further Processing

The iridium-192, scandium-46, and cobalt-60 can be removed easily and without much expense using ion exchange separation techniques. More difficult techniques are

www.manaraa.com

required to remove the remaining impurities – by either reverse phase ion exchange or chromatography separation techniques.

www.manaraa.com

CHAPTER 6

CONCLUSIONS AND FUTURE WORK

The purpose of the radioisotopic analysis of the HFIR produced Pm-147 was to characterize and quantify the isotopic impurities. It is not possible to produce promethium-147, either by the irradiation of Nd-146 or by recycling spent fuel, without the subsequent production of isotopic impurities. The results of the gamma spectra analysis for three samples irradiated in the HFIR at ORNL revealed the presence of ten different isotope impurities. The enrichment of Nd-146 was a critical factor in reducing the presence of impurities, thus increasing the Pm-147 yield. NM-668 (97.5% Nd-146) contained approximately 13% less activity from impurities than samples NM-765T (86.8% Nd-146) and NM-765B (86.8% Nd-146).

Pm-146 and -148 are high energy gamma emitters that, along with the Eu-154, are the highest contributors to the dose rate. These impurities are costly and labor intensive to remove, so shielding must be designed to guard against them. Lead shield thickness of 3.5-inches is recommended to minimize exposure from gamma radiation as analyzed for the work case scenario of constant human contact.

Future work on this project will involve removing all the impurities, with the exception of Pm-146 and -148, from the samples with techniques discussed in this paper. The photon peaks of the purified sample will be analyzed utilizing a gamma spectrometer.

www.manaraa.com

List of References

www.manaraa.com

[1] R.W. McKee, “An Evaluation of the Prospects for Large-Scale Production of Promethium-147”, Pacific Northwest Laboratory, August 1966.

[2] "Discovery of Promethium". *ORNL Review* **36** (1). 2003

[3] H. Flicker, J.J. Loferski, and T.S. Elleman, “Construction of a Promethium-147 Atomic Battery,” IEEE Transactions on Electron Devices, January 1964.

[4] F.F. Knapp, R.A. Boll, S. Mirzadeh, “Chromatographic Extraction with Di(2-Ethylhexyl)Orthophosphoric Acid for Production and Purification of Promethium-147,” U.S. Patent No. 7,435,399 B2, October 14, 2008.

[5] James E. Turner, Atoms, Radiation, and Radiation Protection; WILEY – VCH Verlag GmbH & Co. KGaA, Weinheim - 2nd Edition, 2004.

[6] Oak Ridge National Lab (ORNL) Nuclear Medicine Group (NMG) procedure NMG-49 - *Procedure for the Loading, Testing, Certification, and Irradiation of HFIR Hydraulic Tube Capsules*

[7] ORNL Nuclear Medicine Group (NMG) procedure NMG-52 - *HFIR Irradiation Unit - Helium Leak Test*

[8] F.F. Knapp, R.A. Boll, S. Mirzadeh, “ORNL Nuclear Medicine Program Develops Efficient Method for Separation of Promethium-147 from Reactor-Produced Neodymium-147” Isotope News, Vol. 1, Issue 1, pg 5-7

[9] S. F. Mughabghab, Atlas of Neutron Resonances 5th Edition (BNL-325), 2006

[10] Chart of the Nuclides 16th Edition, Lockheed Martin 2002

[11] Akhil, P., “Nuclear Battery,” MES College of Engineering, 2008.

[12] Ragheb, M., “Radioisotopes Power Production” August 19, 2008.

[13] Gerhart Friedlander and Joseph Kennedy, Nuclear and Radiochemistry; John Wiley & Sons, 1955.

[14] J. Kenneth Shultis, Richard E. Faw, Radiation Shielding, Prentice Hall Inc., 1996.

[15] http://neutrons.ornl.gov/hfir/hfir_experiment.shtml

[16] S.T. Mahmood, S. Mirzadeh, K. Farrell, J.V Pace III, and B.M. Oliver, “Neutron Dosimetry of the HFIR Facility,” ORNL Publication # ORNL-TM-12831

www.manaraa.com

[17] M.A. Garland, S. Mirzadeh, C.W. Alexander, G.J. Hirtz, R.W. Hobbs, G.A. Pertmer, F.F. Knapp Jr., "Neutron Flux Characerization of a Peripheral Target Position in the High Flux Isotope Reactor," Applied Radiation and Isotopes, Vol. 59, pgs. 63-72.

[18] http://archaeometry.missouri.edu/naa_overview.html

[19] Atomic Data and Nuclear Data Tables, Vol. 29. Academic Press Inc., 1983.

[20] Isotopic and Spectrographic Analysis for Neodymium Batch# 161701, ORNL

[21] Isotopic and Spectrographic Analysis for Neodymium Batch# 161730, ORNL

[22] C. Rangacharyulu, S.N. Chaturvedi, G.K. Mehta and N. Nath, *The Decay of* ^{147}Nd, Aust. Journal of Physics, 1974, vol. 27, pgs. 869-77.

[23] S.F. Mughabghab, M. Divadeenam, N.E. Holden, Neutron Cross Sections – Neutron Resonance Parameters and Thermal Cross Sections, Volume 1, Part B, Academic Press, 1981.

[24] http://en.wikipedia.org/wiki/Scandium

[25] George Chabot, "Relationship Between Radionuclide Gamma Emission and Exposure Rate," http://www.hps.org/publicinformation/ate/faqs/gammaandexposure.html

[26] George Chabot, "Shielding of Gamma Radiation," http://www.hps.org/documents/shielding_of_gamma_radiation.pdf

[27] A. Kavetskiy, G. Yakubova, Q. Lin, D. Chan, S.M. Yousaf, K.Bower, J.D. Robertson, A. Garnov, and D. Meier, "Promethium-147 Capacitor," Applied Radiation and Isotopes, Vol. 67 (2009), pgs. 1057-1062.

.

[28] http://www.icrp.org/

[29] Bernard Shleien, The Health Physics and Radiological Health Handbook, Revised Edition, Scinta Inc., 1992.

www.manaraa.com

APPENDICES

www.manaraa.com

Appendix A: Figures

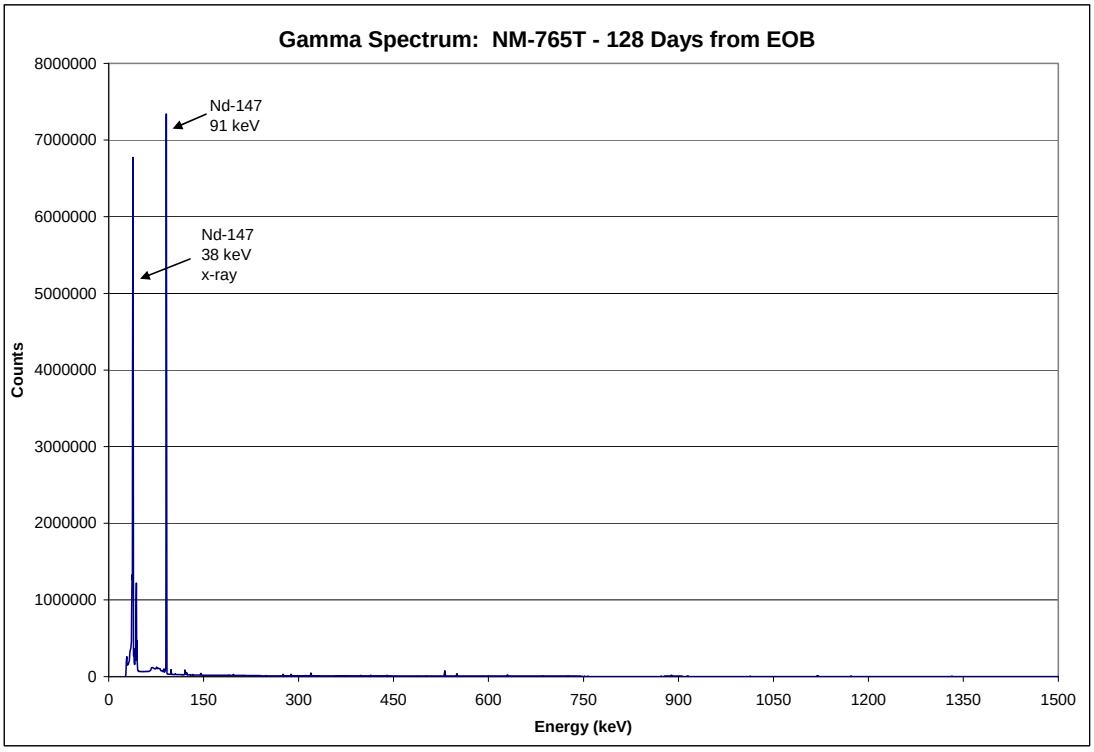

Figure 4.13: Gamma Spectrum of NM-765T

www.manaraa.com

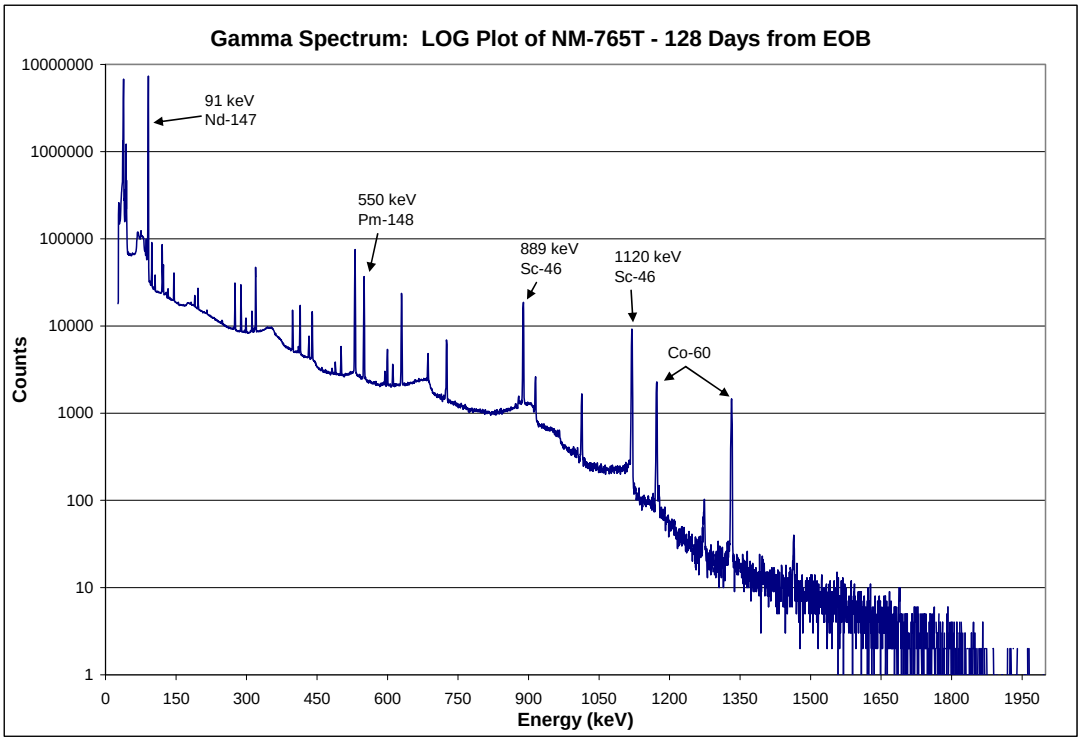

Figure 4.14: Log Plot of Gamma Spectrum for NM-765T

www.manaraa.com

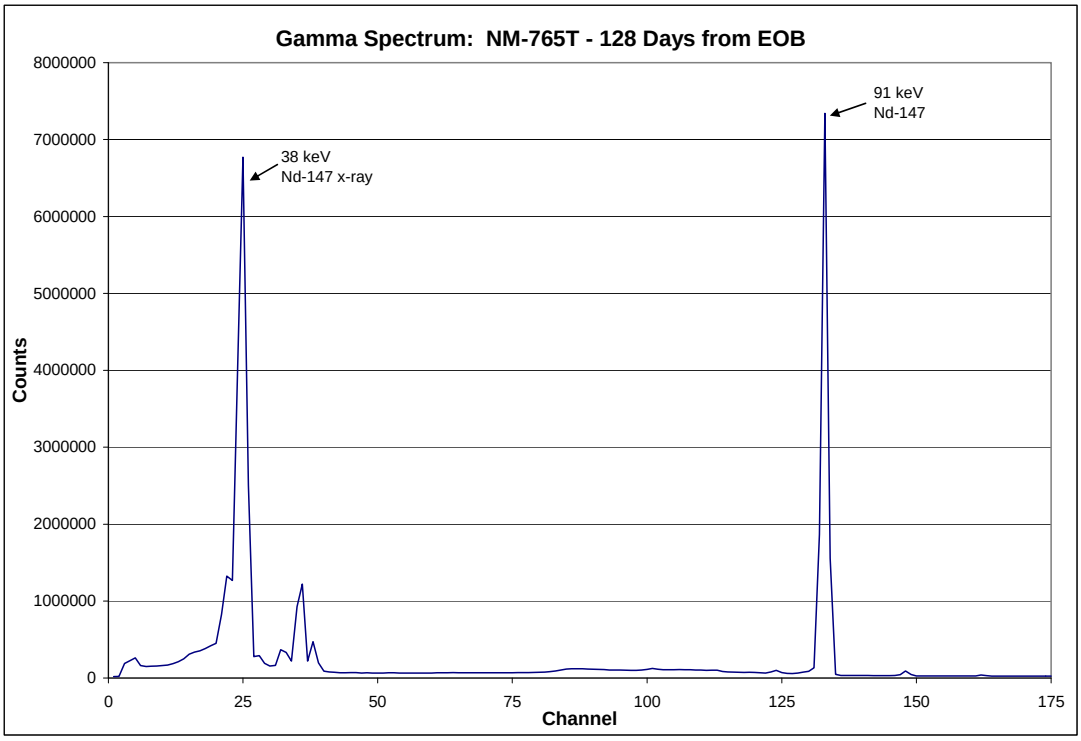

Figure 4.15: Gamma Spectrum: NM-765T – Channel 1–175

www.manaraa.com

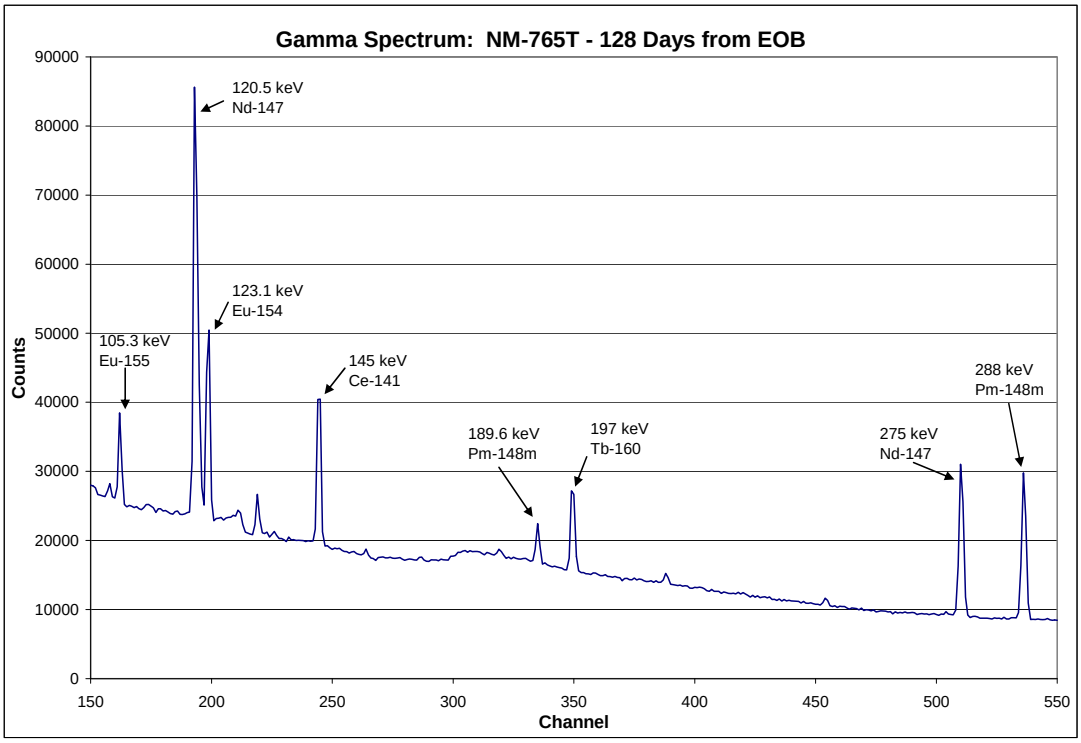

Figure 4.16: Gamma Spectrum: NM-765T – Channel 150-550

www.manaraa.com

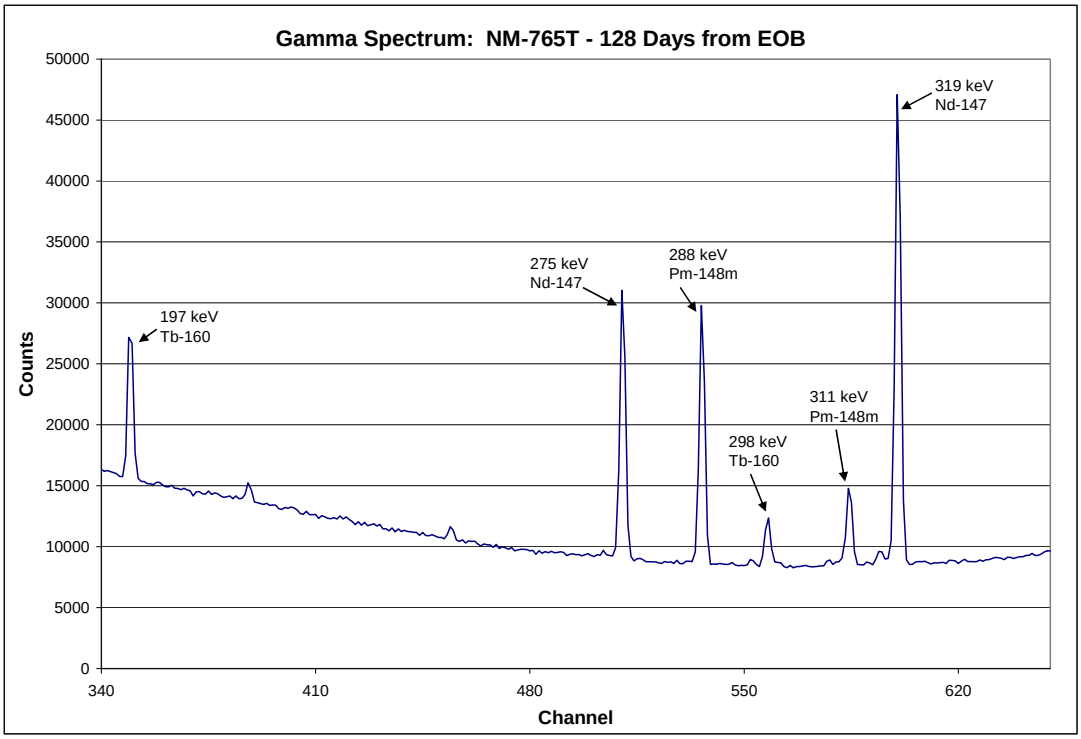

Figure 4.17: Gamma Spectrum: NM-765T – Channel 340-650

www.manaraa.com

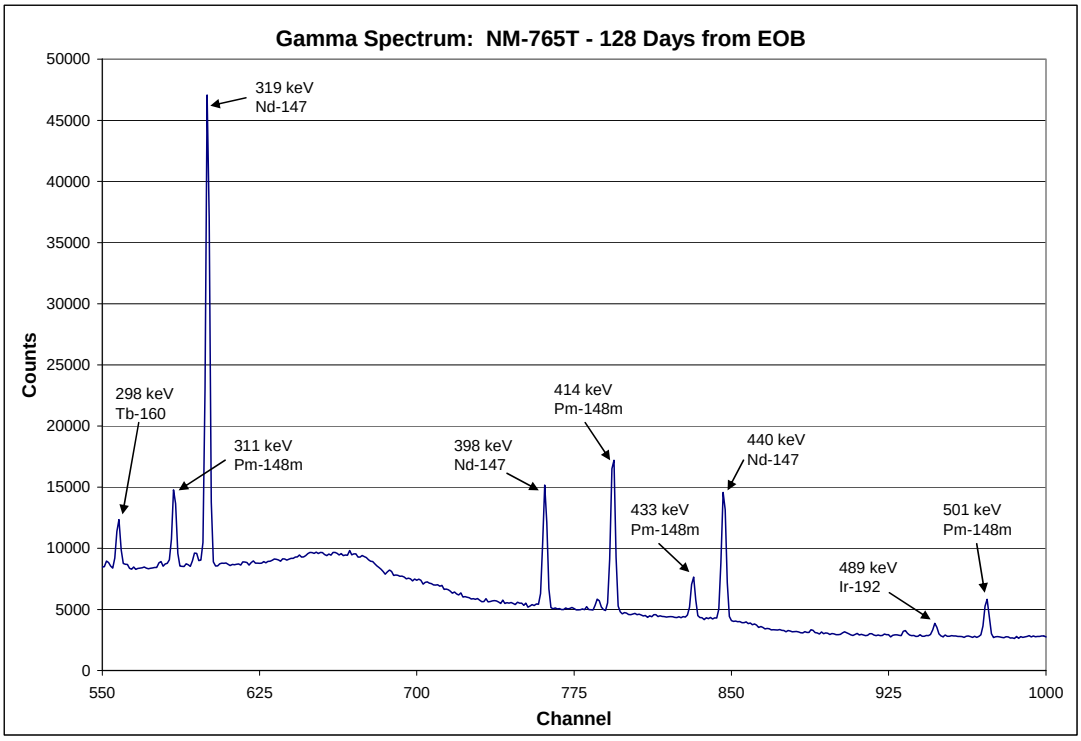

Figure 4.18: Gamma Spectrum: NM-765T – Channel 550-1000

www.manaraa.com

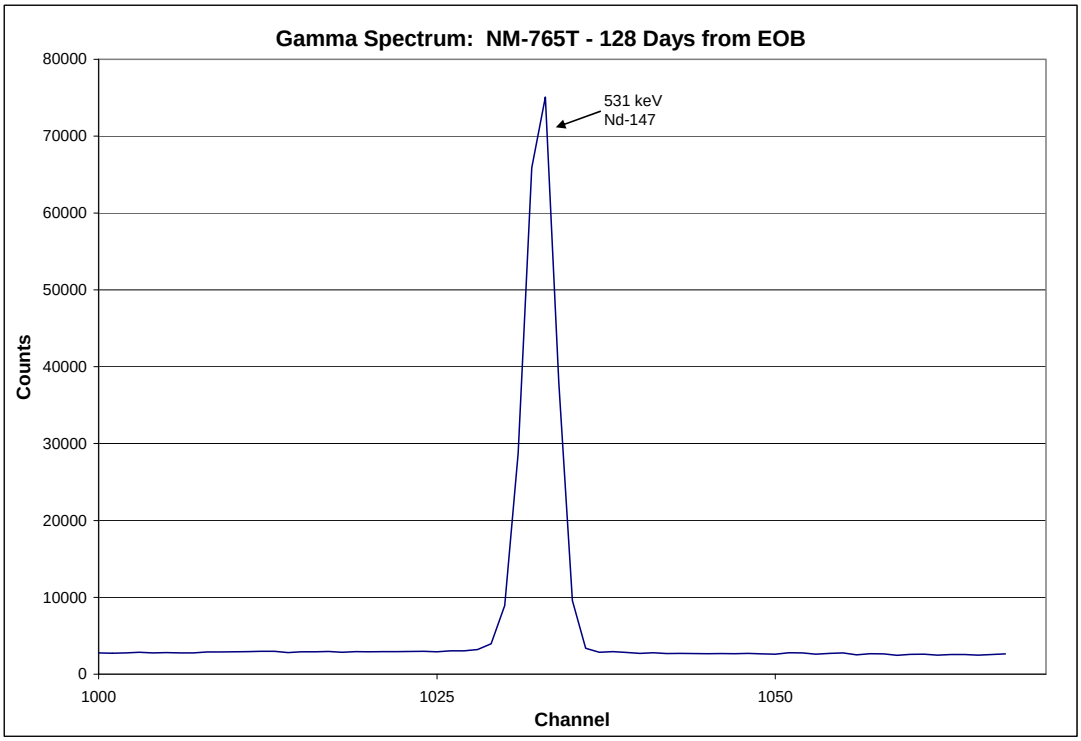

Figure 4.19: Gamma Spectrum: NM-765T – Channel 1002-1069

www.manaraa.com

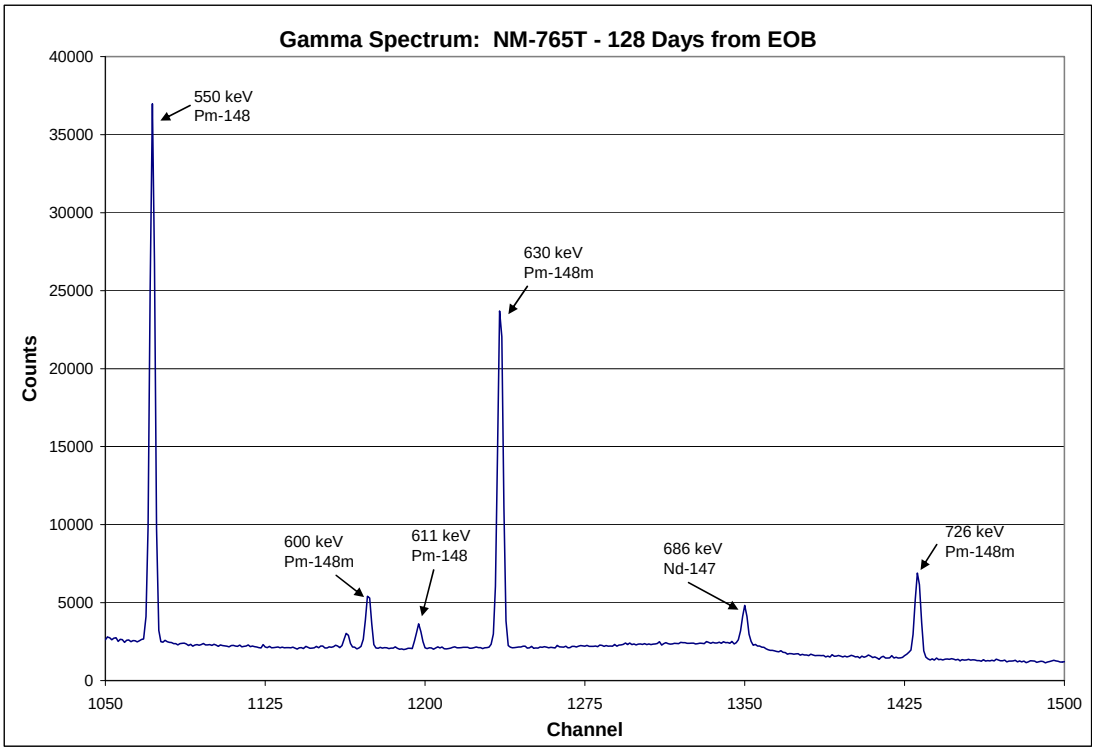

Figure 4.20: Gamma Spectrum: NM-765T – Channel 1052-1502

www.manaraa.com

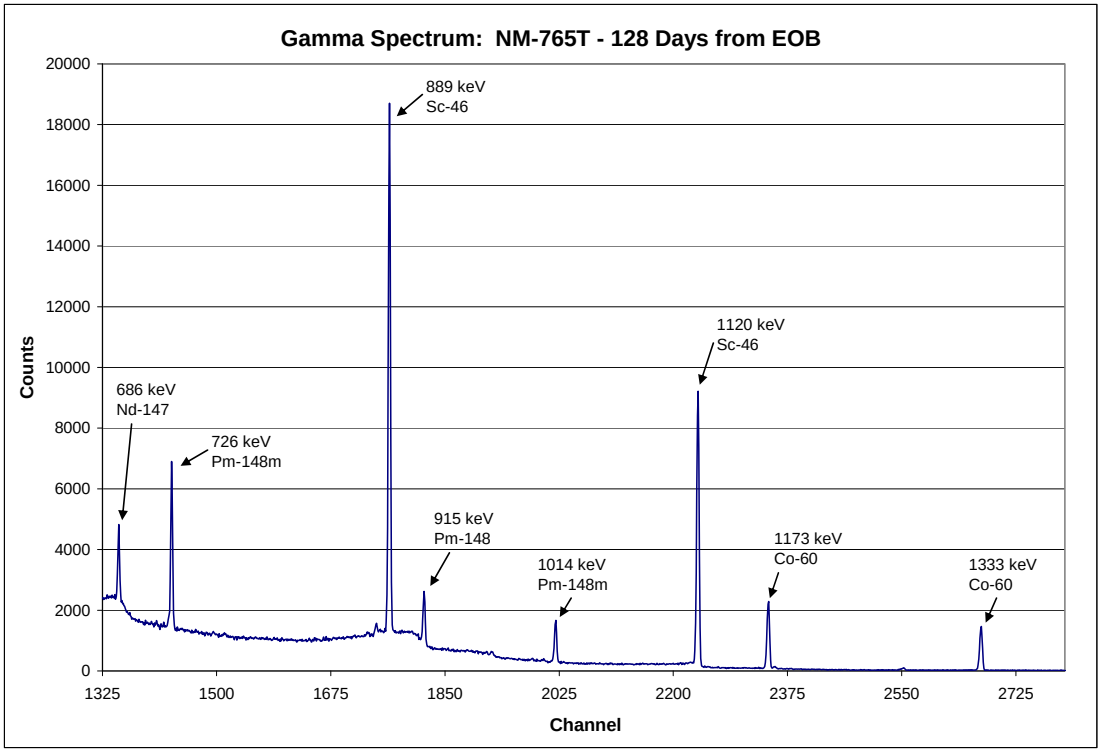

Figure 4.21: Gamma Spectrum: NM-765T – Channel 1353-4097

www.manaraa.com

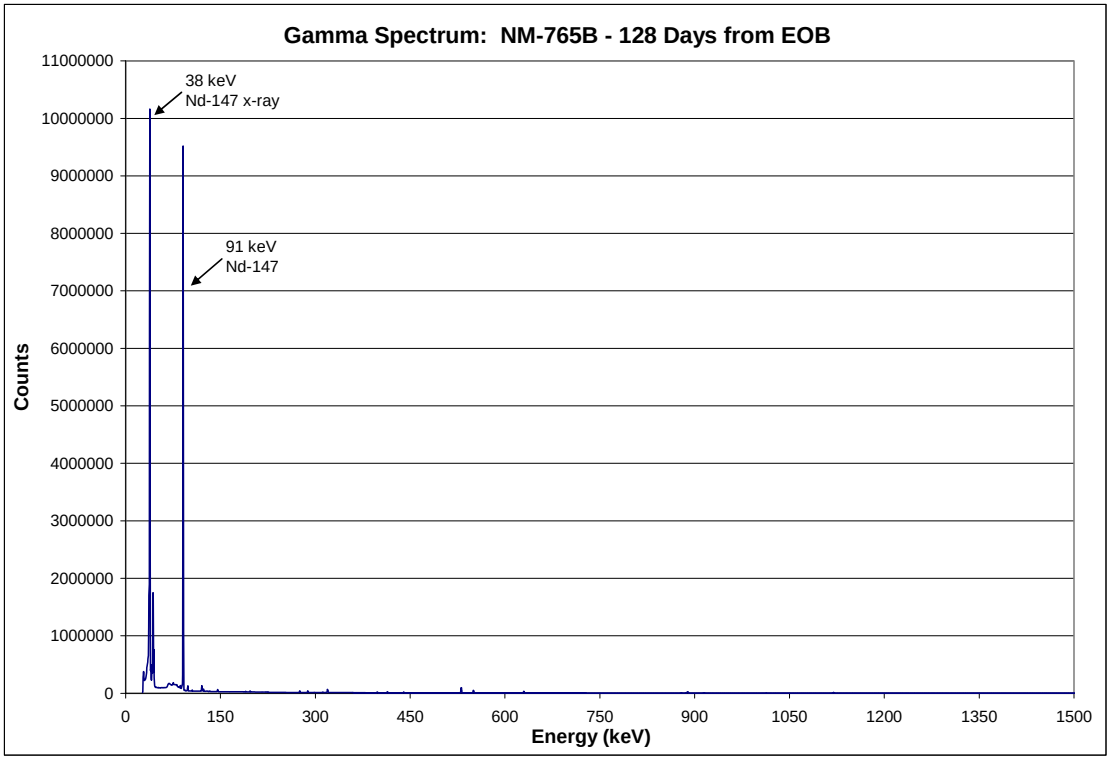

Figure 4.22: Gamma Spectrum of NM-765B

www.manaraa.com

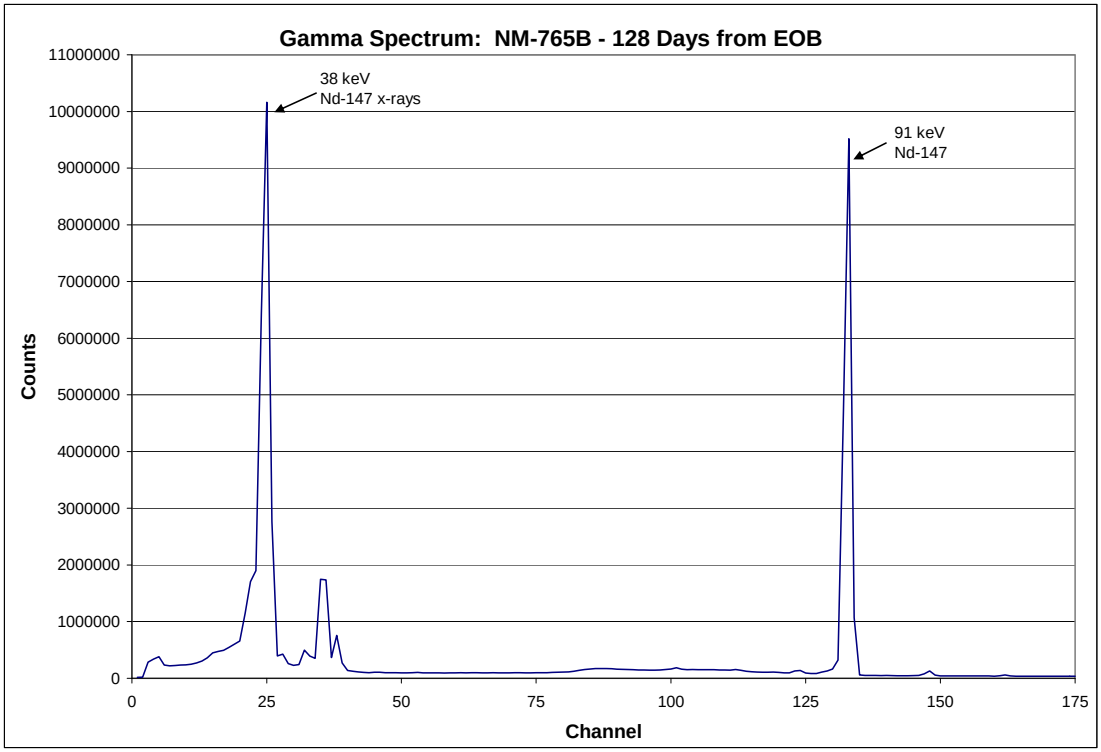

Figure 4.23: Gamma Spectrum: NM-765B – Channel 1 – 175

www.manaraa.com

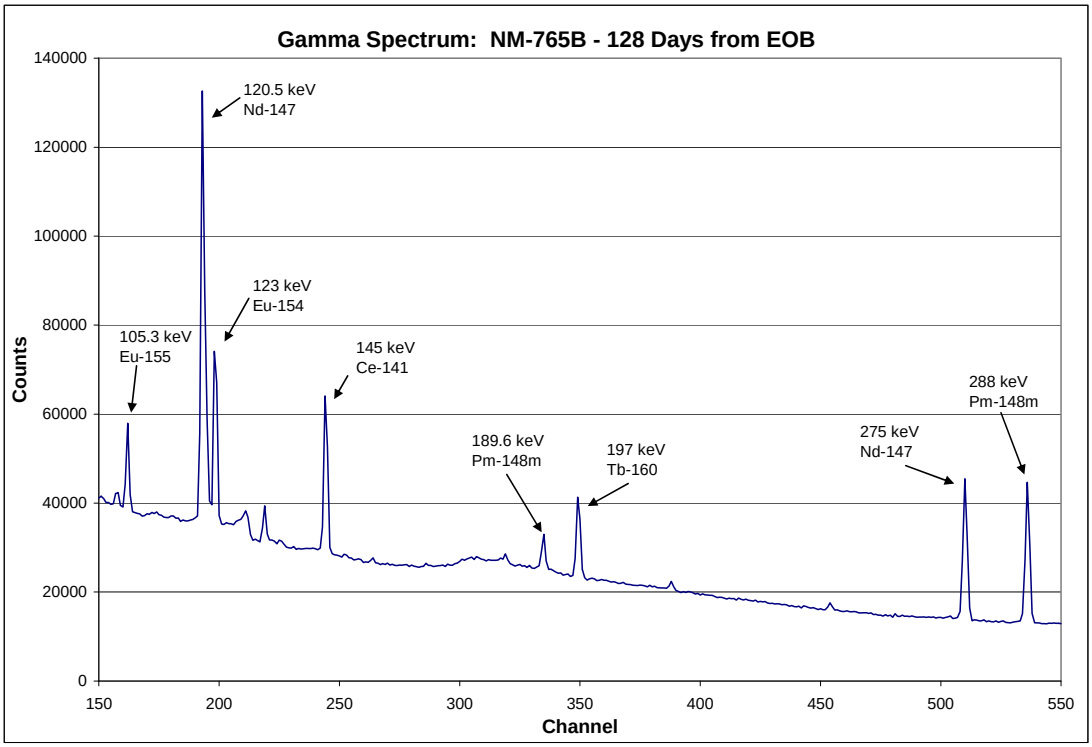

Figure 4.24: Gamma Spectrum: NM-765B – Channel 150-550

www.manaraa.com

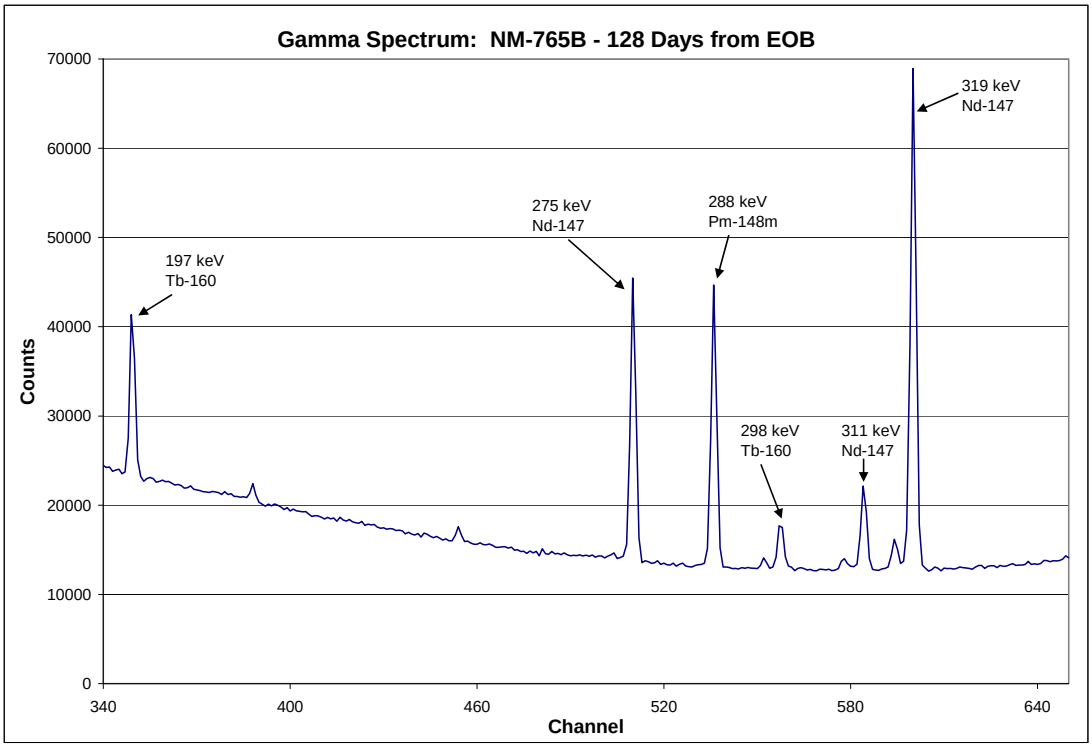

Figure 4.25: Gamma Spectrum: NM-765B – Channel 340-650

www.manaraa.com

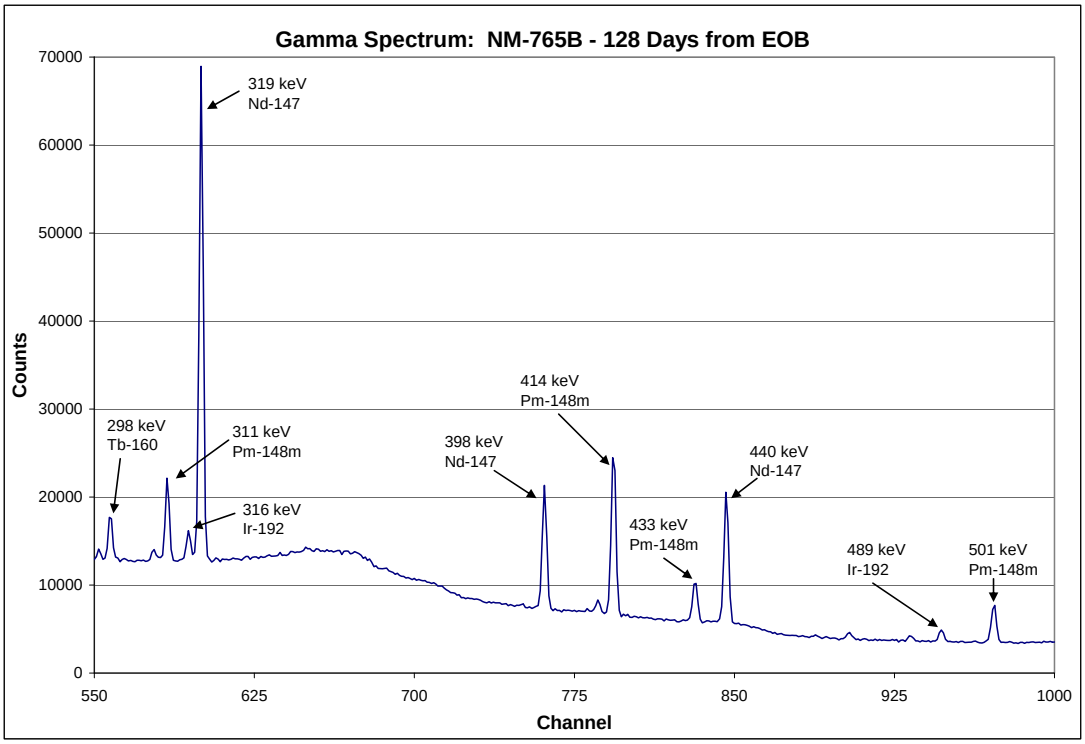

Figure 4.26: Gamma Spectrum: NM-765B – Channel 550-1000

www.manaraa.com

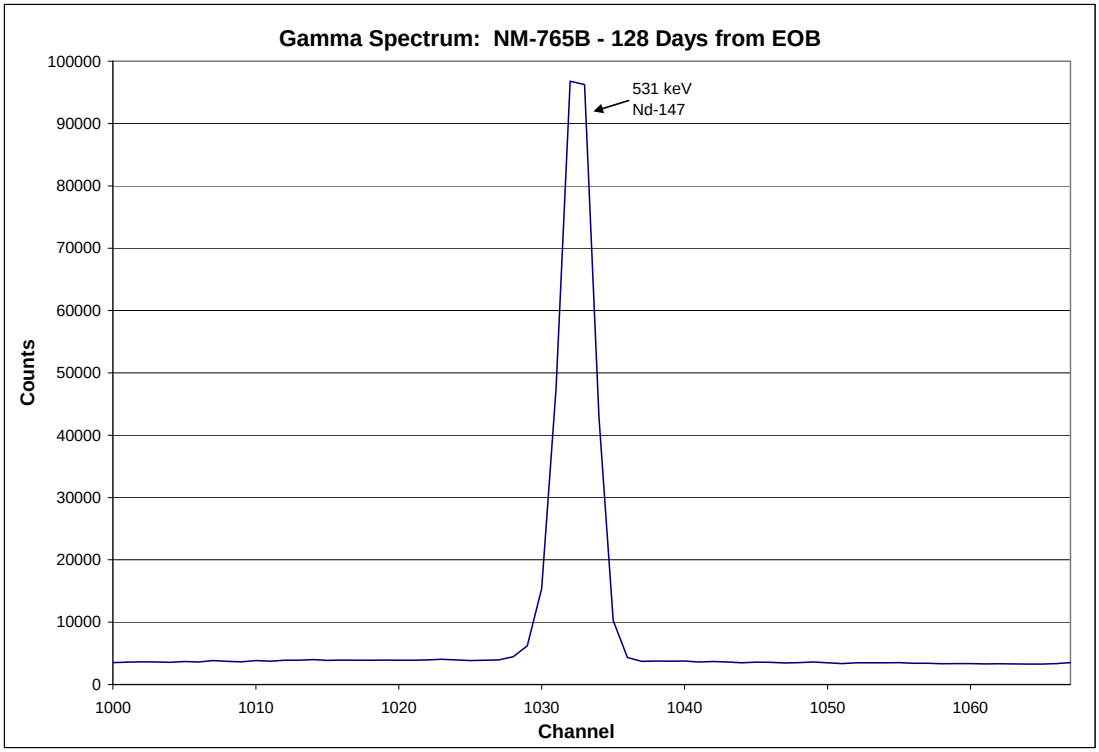

Figure 4.27: Gamma Spectrum: NM-765B – Channel 1000-1070

www.manaraa.com

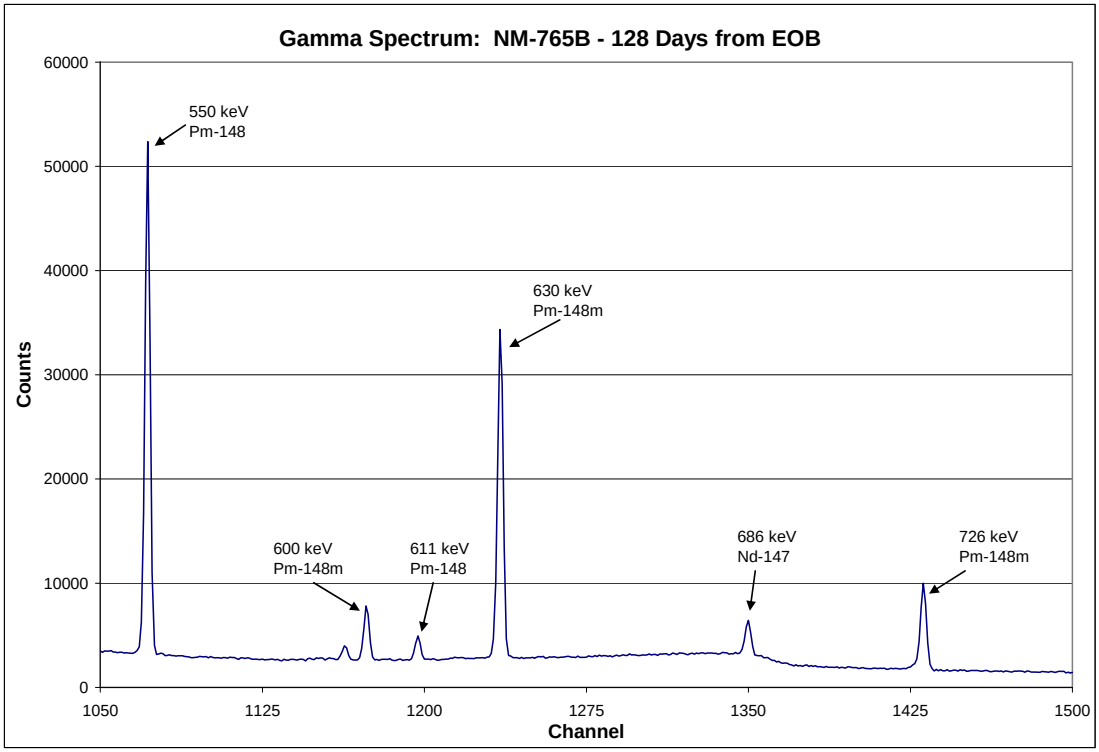

Figure 4.28: Gamma Spectrum: NM-765B – Channel 1050-1500

www.manaraa.com

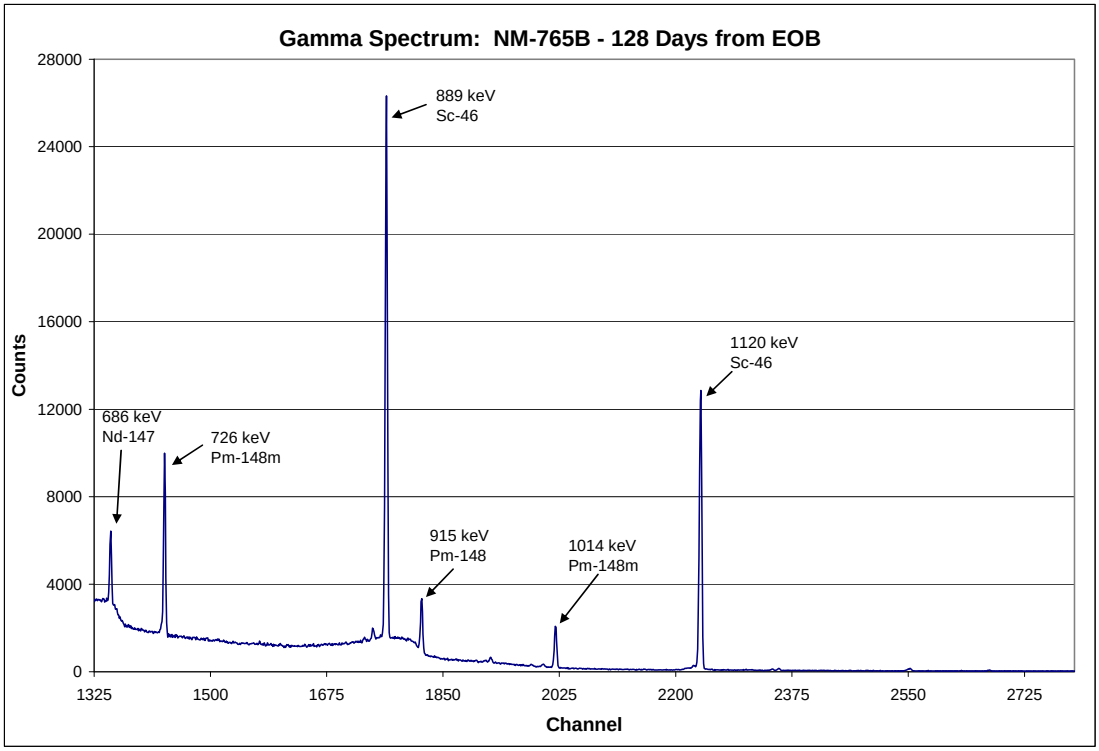

Figure 4.29: Gamma Spectrum: NM-765B – Channel 1350-2800

www.manaraa.com

Appendix B: Tables

Table 4.4: Calculations for Samples NM-765T and -765B Radioactivity

				NM-765T (10cm shelf)			
Radioisotope	Half-life	Gamma used in Counting (keV)	% Intensity	CPS	Shelf Efficiency	Conversion Factor	Radioactivity
Nd-147	10.98 days	91.1	27.9	5.81E+02	1.10E-03	1.14E+01	4.16E+01
Pm-147	2.62 years	121.3	0.0028	nd			nd
Pm-148	41.3 days	550	95.6	5.51	4.60E-05	1.63E+00	2.75E+00
Eu-152	13.3 years	344	26.6	nd			nd
Eu-154	8.8 years	123.1	40.5	3.14	1.70E-03	2.55E+01	1.00E-01
Eu-155	4.68 years	105.3	21.8	1.04	2.02E-02	1.63E+02	5.19E-03
Gd-153	247 days	103.2	21.8	1.30E-01	2.00E-03	1.61E+01	6.55E-03
Ir-192	78.8 days	316	82.9	1.54E-01	4.04E-04	1.24E+01	1.01E-02
Co-60	5.27 years	1173	99.9	5.80E-01	1.85E-05	6.84E-01	6.90E-01
Sc-46	84 days	1120.5	100	2.23E+00	1.80E-05	6.66E-01	2.72E+00
Tb-160	72 days	298.6	27.4	5.87E-01	1.50E-04	1.52E+00	3.14E-01
Ce-141	32.5 days	145	48	2.66E+00	1.25E-03	2.22E+01	9.74E-02

Table 4.5: Calculations for Sample NM-668 Radioactivity

Radioisotope	Half-life	Gamma used in Counting (keV)	% Intensity	CPS	Shelf Efficiency	Conversion Factor	Radioactivity (μCi/mg)
Nd-147	10.98 days	91.1	27.9	1.20E-01	7.80E-03	80.5194	1.60E-02
Pm-147	2.62 years	121.3	0.0028	4.53E-01	6.15E-03	0.0063714	7.65E+02
Pm-148	41.3 days	550	95.6	1	2.45E-03	86.6614	1.24E-01
Eu-152	13.3 years	344	26.6	1.26E-01	5.04E-03	49.60368	2.73E-02
Eu-154	8.8 years	123.1	40.5	5.2	3.74E-02	560.439	9.98E-02
Eu-155	4.68 years	105.3	21.8	1.02	4.48E-02	361.3568	3.04E-02
Gd-153	247 days	103.2	21.8	3.44E-01	4.45E-02	358.937	1.03E-02
Ir-192	78.8 days	316	82.9	4.02E+01	6.80E-03	208.5764	2.07E+00
Co-60	5.27 years	1173	99.9	8.02E-02	4.10E-04	15.15483	5.69E-02
Sc-46	84 days	1120.5	100	1.43E-02	4.40E-04	16.28	9.44E-03
Tb-160	72 days	298.6	27.4	nd	6.00E-03	60.828	nd
						SUM:	7.67E+02

www.manaraa.com

Table 4.6: Shield Calculation Results for NM-668

Lead Thickness (inches)	Dose Rate (mR/hr)
0.25	1.34E+05
0.5	2.02E+04
1	1.81E+03
2	5.95E+01
3	3.66E+00
4	2.91E-01
5	2.63E-02
6	2.55E-03

Table 4.7: Lead Shielding Calculation Parameters for NM-668

Pm-148 Source (Ci)	S (counts/s)		E (MeV)	μ	Shield Thickness, T (cm)	μen/ρ	A1	α1	α2	Distance from Source, r (cm)
1.24E-02	4.37E+08		0.74	1.21	8.89	3.22E-02	2.94	-0.0153	0.127	8.89
Eu-152 Source (Ci)	S		E (MeV)	μ	Shield Thickness, T (cm)	μen/ρ	A1	α1	α2	Distance from Source, r (cm)
2.73E-03	2.69E+07		0.344	0.831	8.89	3.23E-02	1.7	-0.0051	0.185	8.89
Eu-154 Source (Ci)	S		E (MeV)	μ	Shield Thickness, T (cm)	μen/ρ	A1	α1	α2	Distance from Source, r (cm)
9.98E-03	3.42E+08		0.753	0.802	8.89	3.19E-02	2.96	-0.0154	0.126	8.89
Eu-155 Source (Ci)	S		E (MeV)	μ	Shield Thickness, T (cm)	μen/ρ	A1	α1	α2	Distance from Source, r (cm)
3.04E-03	3.71E+07		0.096	28.563	8.89	2.55E-02	0.643	-0.447	-0.647	8.89
Pm-146 Source (Ci)	S		E (MeV)	μ	Shield Thickness, T (cm)	μen/ρ	A1	α1	α2	Distance from Source, r (cm)
2.10E-04	5.05E+06		0.453	1.316	8.89	3.29E-02	2.12	-0.0085	0.141	8.89
Gd-153 Source (Ci)	S		E (MeV)	μ	Shield Thickness, T (cm)	μen/ρ	A1	α1	α2	Distance from Source, r (cm)
1.03E-03	8.38E+06		0.103	79.273	8.89	2.55E-02	0.643	-0.447	-0.647	8.89

www.manaraa.com

Vita

James H. Hinderer was born in 1980 in Murfreesboro, Tennessee. He grew up in Oneida, Tennessee where he graduated from Oneida High School as the class valedictorian in 1999. He attended The University of Tennessee and received his Bachelor's degree in Mechanical Engineering in May 2004. During his undergraduate years, he worked at Mitsubishi Polyester Film in Greenville, South Carolina and at Babcock & Wilcox (B&W) Y-12 National Security Complex in Oak Ridge, Tennessee. He is currently working as an engineer for the National Nuclear Security Administration at the Y-12 Site Office in Oak Ridge, Tennessee.

www.manaraa.com